APPENDIX A

Appendix A provides documentation of additional analyses and testing of the D2/D3 modification which form the basis for extending the operational limits of the forward flushing procedure. The documentation is in the form of updates to sections 8.2.7, 9.0, 9.1 and 9.2.1 of the D2/D3 Design Modification Evaluation Package. These updated sections are designated A8.2.7, A9.0, A9.1 and A9.2.1 respectively.

Section A8.2.7 includes additional discussions of thermal/hydraulic boundary conditions and film coefficients which are the basis for the additional structural analysis for which results are presented in Sections A9.0, A9.1 and A9.2.1.

The sections in this Appendix are alternates to the respective sections in the main body of the evaluation package. Either provides an acceptable basis for the adequacy of the D2/D3 modification for plant operation within the corresponding specified limits.

Areas where the sections of Appendix A differ from the corresponding sections in the main body of the package are indicated with vertical lines in the right margin of the page.

0775c/0112c/041183:5 1

A8.2-7 Heat Transfer Coefficients

Heat transfer coefficients for the Model D2/D3 steam generator preheater modification have been determined for stress analysis. The heat transfer coefficients were calculated using conservative correlations for forced convection and natural convection.

Film coefficients based on forced convection were calculated for temperatures ranging from 32°F to 430°F and velocities ranging from no flow to 30 ft/sec. Typical calculational results for the internal manifold inlet and exit plate downstream surfaces are shown in Figure A8.2-26. The film coefficients shown in Figure A8.2-26 were calculated using a correlation based on forced convection for flow parallel to a plane (Reference A8.2-6, equation 9-41).

Several aspects of the application of heat transfer coefficients for the forward flushing event are presented in mora detail here because of the high thermal induced loads which result in the internal manifold.

Manifold Entrance and Exit Plates

The temperatures in the entrance and exit plates are influenced by heat transfer within the holes as well as on the plate upstream and downstream surfaces. The bulk fluid temperature within the holes was conservatively assumed [.]a,c,e This assumption was corroborated with an experiment which included measuring fluid temperatures in a hole of a simulated manifold plate. Figure A8.2-27 shows the location of the thermocouples on the plate. Figures A8.2-28 and A8.2-29 illustrate the results of the experiment. These show that over the range of Richardson numbers (based on both the velocity and temperature difference between upstream and downstream) applicable to the 1-1/2 percent forward flushing case, [

.]a,c,e This effect would be even

less pronounced for higher forward flushing rates. The conclusion was that in the computation of metal temperatures for the entrance and exit plates, it is conservative to assume that[

]a,c,e

Heat transfer coefficients were developed for use in the WECAN thermal model which considered the entrance and exit plate as a solid structure (no holes). This development was done in two steps. First, 3D conduction models were generated for the exit and entrance plate hole geometries. A typical model is shown in Figure A8.2-30. From this model, average metal temperatures as well as surface temperatures were computed for each region of the manifold box plates exposed to different upstream and downstream temperatures. The heat transfer coefficients used in this analysis were determined as follows.

- For the holes, the Ditters-Boelter correlation (reference A8.2-6), with a factor to account for the entrance effect was used.

  $$Nu = 0.023\ (Re)^{0.8}\ (Pr)^{0.4}\ F$$

  where $F = 1.11\ [(Re)^{0.2}/(L/D)^{0.8}]^{0.275}$

  Nu = Nusselt number
  Re = Reynolds number
  Pr = Prandel number
  L = Plate thickness
  D = Hole diameter

- For the upstream and downstream surfaces, the free convection correlation, (Reference A8.2-6, eq. 7-4a) was used.

  $$h = 0.13\ \frac{K_f}{L}\ [Gr\ Pr]^{1/3}$$

  where K_f = fluid conductivity

  Gr = Grashof number
  Pr = Prandtl number
  L = Length (Height)

A sensitivity study was done to assess the influence of the possible uncertainties in these coefficients on the metal temperatures. A summary of the results for the 2.2 percent flow is given in Table A8.2-2. [

]a,c,e The change in upstream (cold side) to downstream (hot side) temperature differences are even smaller.

After determining average and surface plate temperatures, the second step was to compute heat transfer coefficients for use with the WECAN thermal model (solid plate) that would produce the same through-wall gradient and average metal temperature as determined from the 3D model. The result is schematically illustrated in Figure A8.2-31.

Manifold Support Cylinder/Thermal Liner Weld

The other critical area, from a structural standpoint, is the manifold support cylinder to nozzle thermal liner attachment weld. The outside (O.D.) of the nozzle thermal liner is exposed to the water in the downcomer (the annulus formed by the wrapper and the outer steam generator shell). The I.D. of the liner and of the manifold support cylinder are exposed to the incoming feedwater flow. During forward flushing, this flow is stratified, with 32°F water on the bottom and 557°F water on the top. To determine the temperature distributions on these parts with the WECAN thermal model, appropriate heat transfer coefficients were computed for the three areas shown in Figure A8.2.-32.

The heat transfer coefficient used for the O.D. of the nozzle thermal liner, h_3, was computed using the Churchill and Bernstein correlation (Reference A8.2-8)

$$Nu = 0.3 + \frac{0.62\ Re^{1/2} Pr^{1/3}}{\left[1 + \left(\frac{4}{Pr}\right)^{2/3}\right]^{3/4}} \left[1 + \left(\frac{Re}{282000}\right)^{5/8}\right]^{4/5}$$

This correlation is for forced convection over an infinite cylinder. It was assumed that for the area in the liner to nozzle annulus, adjacent to the support cylinder to liner attachment weld, that the Reynolds number would be [

]^{a,c,e}

The heat transfer coefficient across the [ ]^{a,c,e} gap between the support cylinder and the nozzle liner (h_2 in Figure A8.2-32) was based on an "equivalent heat conductivity, Ke", which accounts for the contribution of free convection in the gap to the total heat flow. Figure 11-14 of Reference A8.2.-9 gives a plot of log Ke/K vs. log $Gr_b Pr$. The contribution of convection depends upon the difference between the temperature on the I.D. of the nozzle liner and the O.D. of the manifold support sleeve. When the temperature difference is small, Ke/K = 1. When the temperature difference was a maximum, Ke/K became as high as [ ]^{a,c,e} Values for an equivalent h were defined for 3 axial locations and at every 15° interval around the circumference of the gap for use in the WECAN thermal model.

The film coefficients in the feedwater region (h_1 in Figure A8.2.-32) were based on free convection. This was determined following a comparison of free vs forced convection coefficients. As in the case of the gap coefficients, the coefficients on the inside of the liner and manifold support cylinder were determined for twleve circumferential locations (15° intervals) for three different axial locations. The individual 15° sectors were categorized as near horizontal, near vertical, or diagonal members and the following correlations were used. (Reference A8.2-10).

For vertical sectors,

$$h = 0.13 \frac{K}{L} (Gr\ Pr)^{1/3} \text{ for } Gr > 10^9$$

$$h = 0.555 \frac{K}{L} (Gr\ Pr)^{1/4} \text{ for } 10 < GrPr < 10^9$$

For horizontal sectors

$$h = 0.14 \frac{K}{L} (Gr\ Pr)^{1/3} \text{ for } 2 \times 10^7 < Gr < 3 \times 10^{10}$$

and

$$h = 0.54 \frac{K}{L} (Gr\ Pr)^{1/4} \text{ for } 10^5 < Gr < 2 \times 10^7$$

For diagonal sectors, h was determined as the average of the horizontal and vertical values. Grashof numbers were generally $> 10^9$.

Since these free convection coefficients depend upon the fluid to surface temperature difference, it was necessary to perform iterative calculations with the WECAN thermal model to arrive at a "final" set of h_1 values.

The temperature difference between the mid-wall locations in the support cylinder and the thermal liner near the weld (at the bottom or coldest location around the circumference) was computed to be[ ]a,c,e A study was performed to assess the sensitivity of support cylinder mid wall to nozzle liner mid wall temperature difference to variations in values of h_1, h_2 and h_3. The results are shown in Figure A8.2-33. [.]a,c,e Note that the range in the ΔT is different from the range that may be inferred from the ranges in the individual mid-wall temperatures. This is because of the fact that the maximum and minimum temperatures for the liner and support sleeve mid wall points occur for different combinations of values of h_1, h_2 and h_3.

During the forward flushing transient striping occurs in the steam generator main feedwater nozzle and preheater inlet region. This was determined from tests conducted at WARD on a 0.45 scale plexiglass model (Section 8.2.5). The heat transfer process of the stratified flow can be separated into three region; lower cold water zone, upper hot water zone, and interface thin layer. The film coefficient for the thin interface layer where thermal striping occurs is[

]a,c,e

References

A8.2-6 N. H. McAdams "Heat Transmission" Third Ed., 1954.

A8.2-7 H. Choe and C. M. Kwong, "Turbulent Temperature Fluctuation and Heat Transfer to a Metal Surface Resulting from the Mixing of Cold and Hot Water, ASME Paper No. 79-WA/HT-23, 1979".

A8.2-8 J. P. Holman, Heat Transfer, McGraw Hill, New York, 1981.

A8.2-9 E. R. G. Eckert, Heat and Mass Transfer, McGraw Hill, NY, 1959.

A8.2-10 F. Kreith, Principals of Heat Transfer, IEP, NY 1976.

TABLE A8.2-2

SENSITIVITY STUDY - RESULTS SUMMARY

ENTRANCE PLATE - 2.2% FLOW

b,c,e

LOCATION (BOX/ SECTION)
MIDDLE/6
LOWER/4
LOWER/5
LOWER/6

AVERAGE METAL TEMPERATURES, °F

AVERAGE -HOLE SURFACE

AVERAGE -DOWNSTREAM

AVERAGE -UPSTREAM

FIGURE A8.2-26

FILM COEFFICIENT FOR INTERNAL MANIFOLD
INLET AND EXIT PLATE
DOWNSTREAM SURFACE

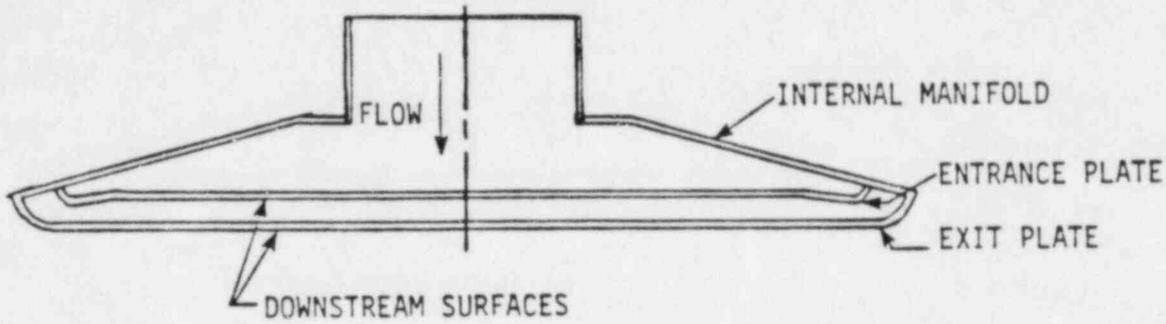

a,c,e

HEAT TRANSFER COEFFICIENT, BTU/HR - FT^2 - °F

APPROACH VELOCITY (ft/sec)

FIGURE A8.2-27

THERMOCOUPLE LOCATIONS

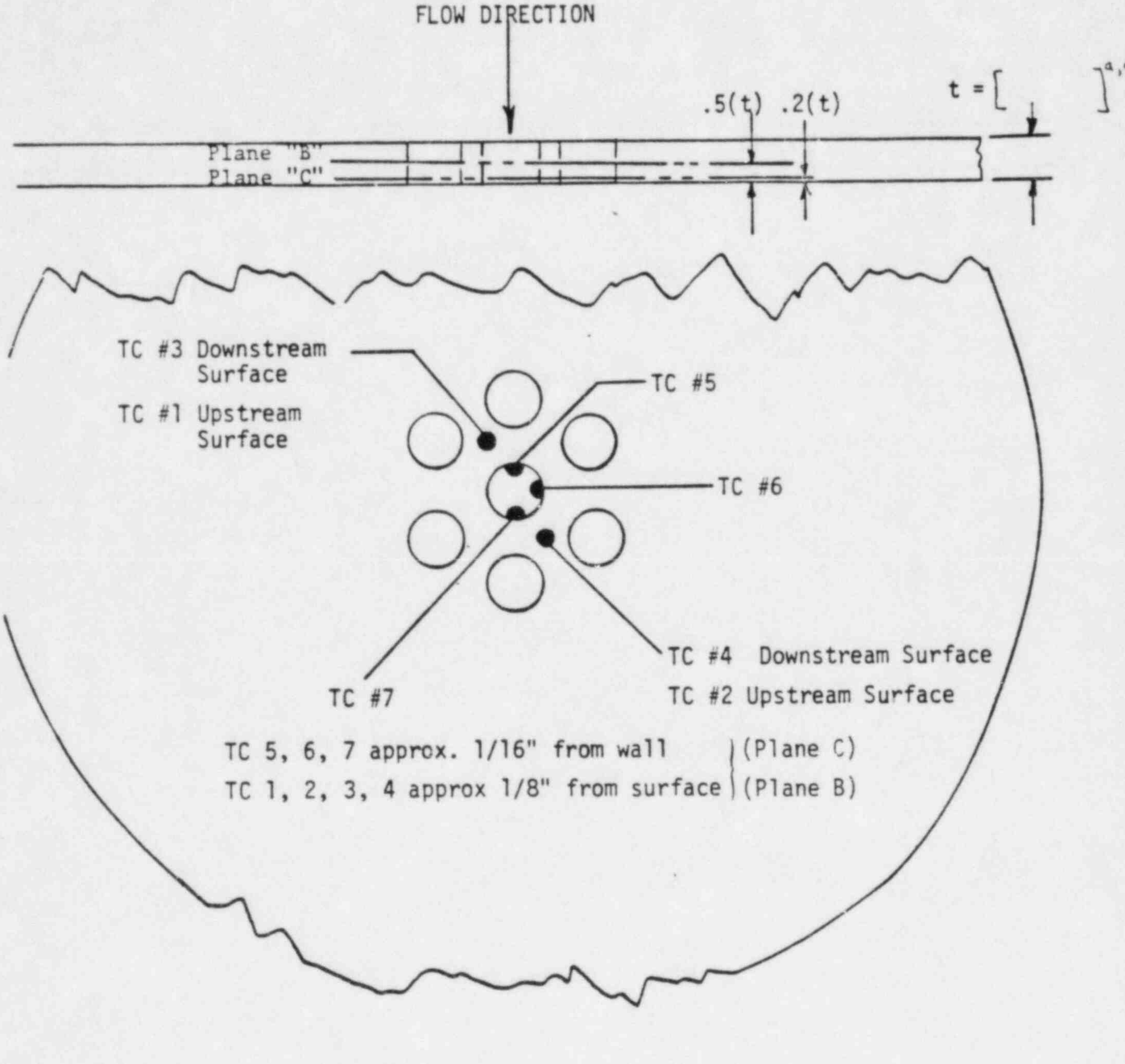

FIGURE A8.2-28

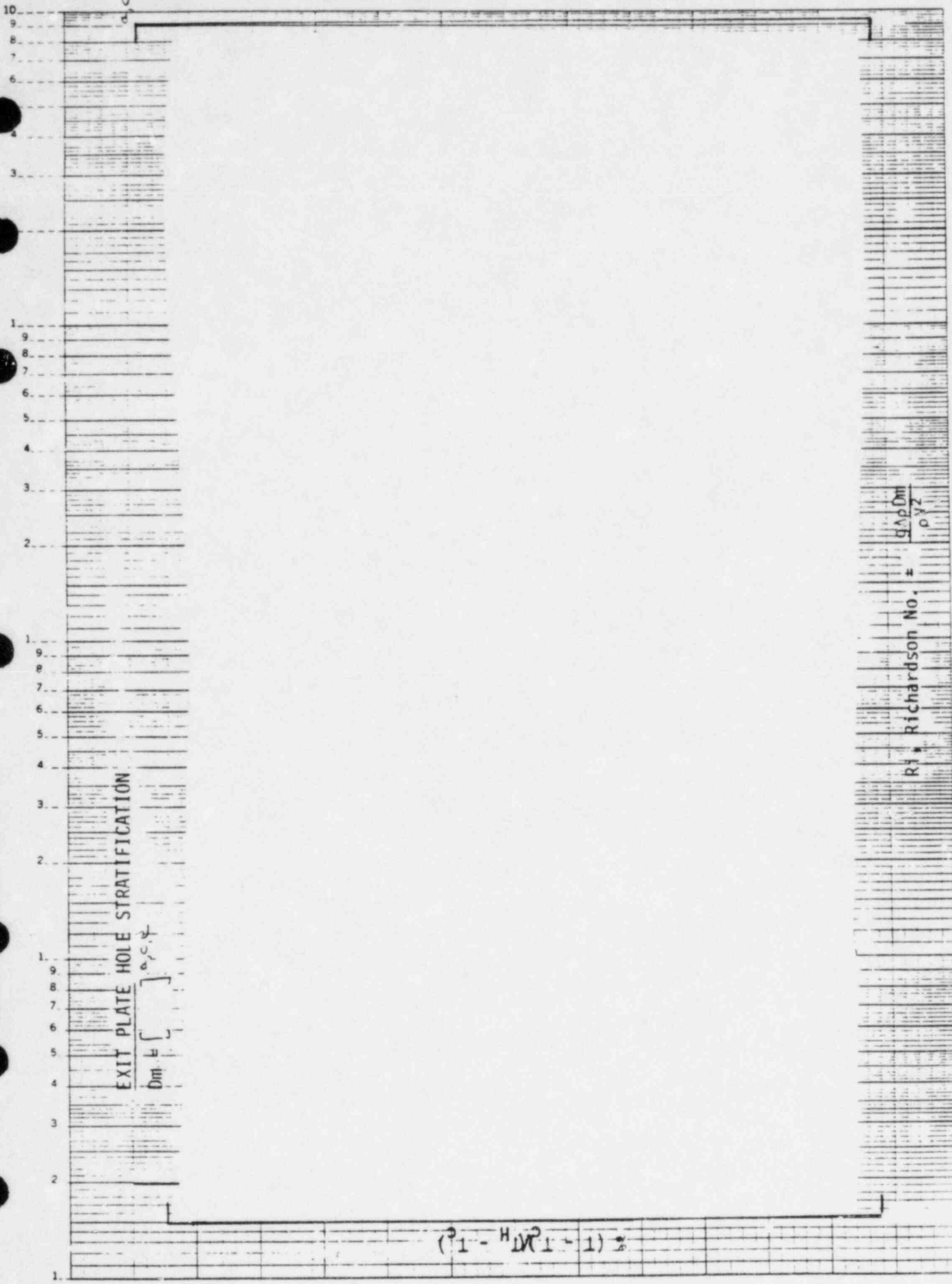

FIGURE A8.2-29

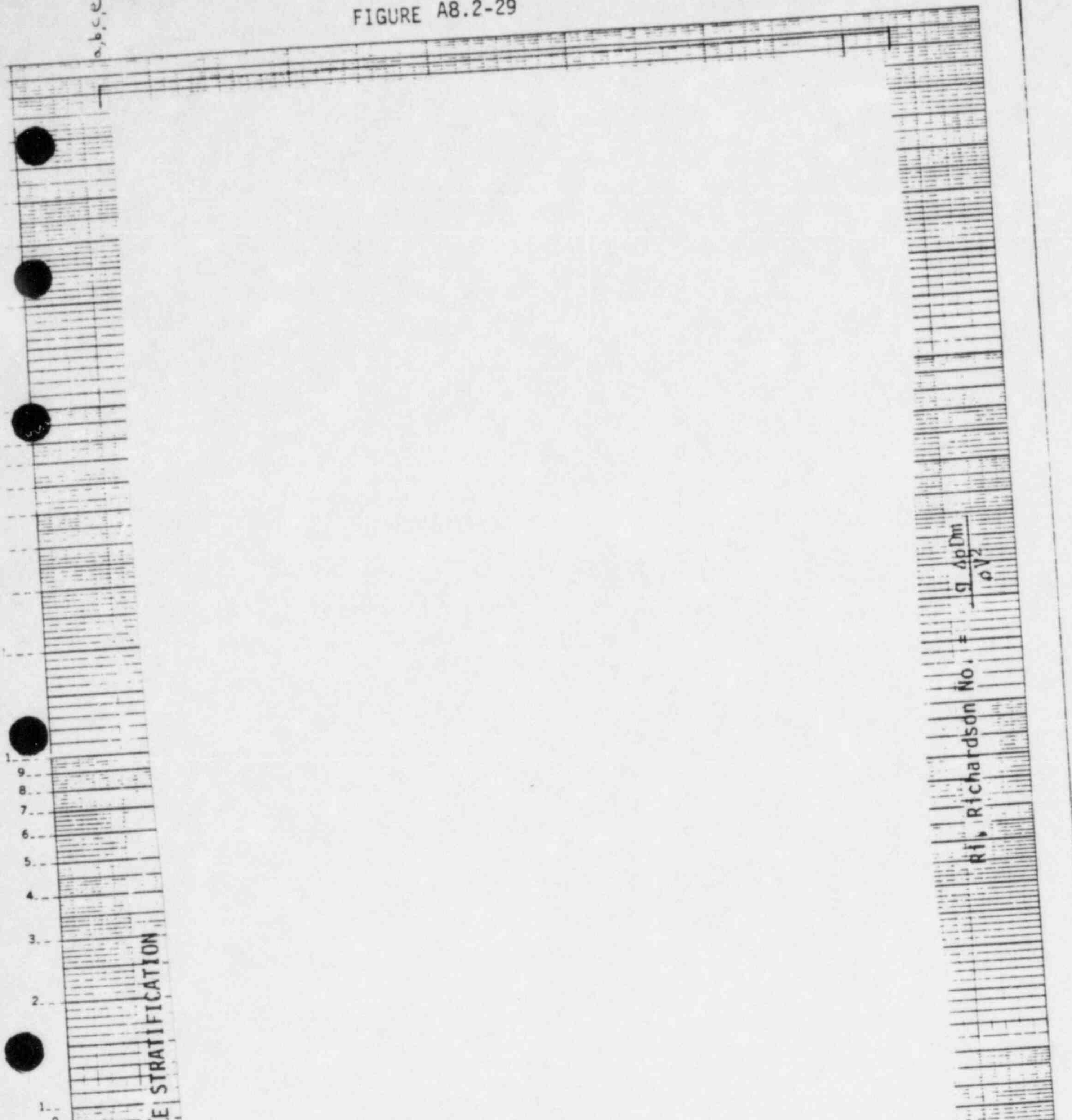

FIGURE A8.2-30

a,c,e

FIGURE A8.2-31

TEMPERATURE CALCS FOR EXIT AND ENTRANCE PLATES

a,c,e

TEMPERATURE CALCS RESULT
IN EQUAL METAL TEMPERATURES
AND EQUAL GRADIENTS

FIGURE A8.2-32

CRITICAL FILM COEFFICIENTS EVALUATED FOR MANIFOLD SUPPORT SLEEVE WELD ANALYSIS

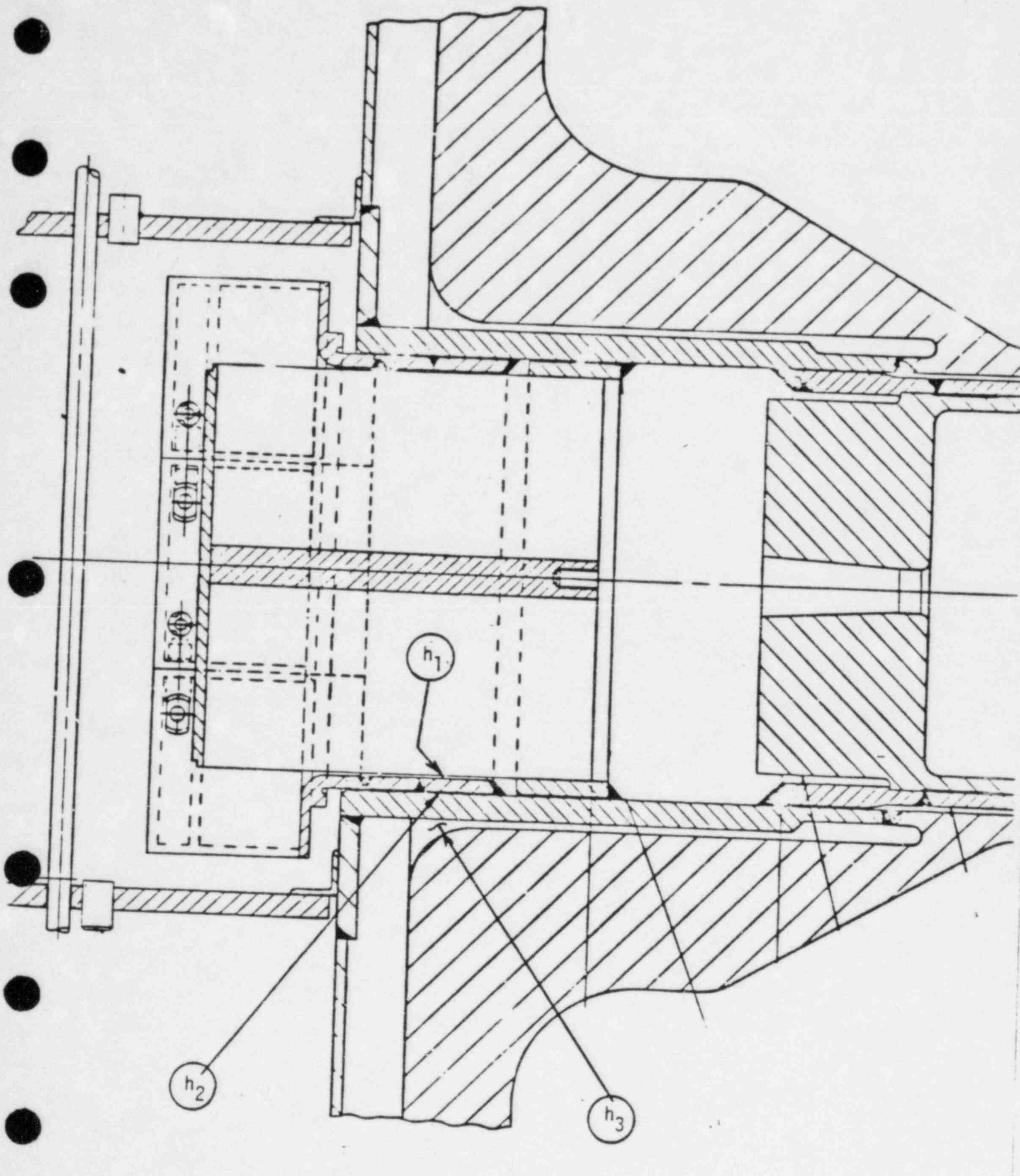

FIGURE A8.2-33

EFFECT OF FILM COEFFICIENT UNCERTAINTY

a,c,e

Section A9.0

STRUCTURAL ANALYSIS

A9.0 STRUCTURAL ANALYSIS

The Model D2 and D3 Preheat Steam Generator Manifold Modification, Flow Splitter and Nineteen-hole Reverse Flow Limiter have been evaluated to demonstrate their structural integrity for the expected service conditions for a forty year period. This has been accomplished through the use of conventional mechanics analysis, matrix methods, and several stages of detailed finite element analysis to establish stress states for stress and fatigue evaluation. All of the mechanical load, pressure and thermal transient conditions described in Section 8.0 have been assessed to the guidelines of the criteria of the ASME Boiler and Pressure Vessel Code, Section III, Subsections NB and NG. This criteria has been supplemented when needed by plastic-dynamic analysis and crack propagation analysis (Section 10.0) to confirm the integrity of critical regions. Summary tables are provided in each subsection of Section 9 presenting results for the most critical sections of each component for primary and secondary stresses and fatigue usage.

Of the loading conditions that were included in the evaluations of the modification, the forward flushing transient, which results in stratification in the manifold, was the most limiting. The structural evaluation contained herein considers forward flushing purge rates of 1.5 percent, 2.2 percent and 2.7 percent of nominal feedwater flow rate. Forward flushing is considered to occur with purge flow rates from 1.5 percent to 3.0 percent of nominal feedwater flow rate and to result in established stratified flow one time per startup cycle (2050 cycles, total). Forward flushing is intended to purge cold water from the main feedwater line between the steam generator and the main feedwater isolation valve at a low flow rate to minimize the potential for bubble collapse and consequent pressure loading in the steam generator preheater region. The bubble collapse limits on the purge rate and temperature of the main feedwater have previously been established to be $\leq$ 3 percent or $\geq$ 250°F, respectively. In some situations the main feedwater cools to ambient temperatures, which are assumed to be as low as 32°F while the steam generator is at operating temperatures as high as 557°F. The low flow rates during forward flushing give rise to stratification in the main feedwater nozzle region and also in the manifold. The stratified temperature distribution results in high thermal stresses in these areas. A lower limit on the purge flow rate is therefore dictated by structural integrity considerations. Further, the upper purge flow limit (3.0 percent) established for bubble collapse considerations must be demonstrated as structurally acceptable with the addition of the modification.

All regions of the modification have been shown to be structurally adequate for the flushing flow rates analyzed and a minimum feedwater temperature of 32°F. For the flow splitter liner weld, usages exceeding unity have been demonstrated to be acceptable based on fatigue crack growth predictions. Further, a major portion of the fatigue usage at this weld is associated with assumed daily load follow and would drop to less than unity if load follow occurred every other day.

Figure A9.0-1 indicates the acceptable limits for temperature and purge flow rate for forward flushing. For the upper bound flow of 3 percent from the bubble collapse considerations, the structural response at flows up to 2.7 percent are extrapolated to obtain the structural behavior at 3 percent flushing flow. [

]a,c,e

[ ]a,c,e

a,c,e

;

a,c,e

FIGURE A9.0-1 Temperature/Flow Rate Guidelines for Forward Flushing

A9.1 Manifold Structural Analysis

A9.1.1 Introduction

This section of the report presents the analyses which have been performed as structural verification of the manifold design modification. The flow splitter and flow limiter components, which are structurally non-integral but functionally related components, are treated on an individual basis in Sections A9.2.1, 9.2.2, 9.2.3 and 9.3.

The analyses presented have been performed predominantly through the use of finite element analysis. The WECAN and ANSYS Computer Codes, References (A9.1-1) and (A9.1-2), respectively, are the principal codes which have been used.

The material properties, the mechanical loads and thermal conditions, and the structural criteria used in the various manifold analyses are discussed in Sections A9.1.2, A9.1.3, and A9.1.4, respectively. An overview of the manifold analysis, describing the interaction between the overall manifold analyses and the detailed analyses, is provided in Section A9.1.5. The interaction analyses between the various manifold boxes for mechanical loads and thermal conditions are discussed in Sections A9.1.6 and A9.1.7 respectively. The detailed structural analyses of Section A9.1.8 through A9.1.11 deal with localized regions of the manifold which are the critical areas of the manifold. The critical areas were selected based on a preliminary structural evaluation of the top manifold section and engineering judgement. The manifold box interaction analysis was used to verify the selection of these areas for more detailed analysis. Finally, a detailed analysis of the top/bottom plate of the manifold boxes in the vicinity of the vertical bolts joining the boxes is contained in Section A9.1.12.

A9.1.2 Material Properties

The material properties for the analysis of the manifold are taken from the ASME Code, Section III, Reference (A9.1-3). A summary of the structural materials by component is given in Table A9.1.2-1. The corresponding material properties are given in Table A9.1.2-2 at a temperature of 440°F. Except for Poisson's ratio, temperature dependent material properties have been used for the structural analyses.

In a number of the structural analyses which follow, a part of the structural model has approximated one or more perforated plates using equivalent solid plate properties. Due to the various plate porosities in different regions within the manifold, the equivalent plate properties will be provided as a part of the detailed analysis descriptions.

TABLE A9.1.2-1

SUMMARY OF STRUCTURAL MATERIALS

a,c,e

COMPONENT	MATERIAL

TABLE A9.1.2-2

SUMMARY OF MATERIAL PROPERTIES[1]

a,c,e

MATERIAL PROPERTY	
YOUNG'S MODULUS (PSI)	
DENSITY ($LB\text{-}SEC^2/IN^4$)	
COEFF. OF THERMAL EXPANSION-/°F	
POISSON'S RATIO	
CONDUCTIVITY-BTU/IN-SEC-°F	
SPECIFIC HEAT- BTU-IN/LB-SEC^2-°F	

(1) MATERIAL PROPERTIES AT 440°F.

A9.1.3 Summary of Loading Conditions

A9.1.3.1 Mechanical Loads

Mechanical loads are imposed on the manifold through three generic mechanisms. These mechanisms are earthquakes, waterhammer pressure oscillations, and steady-state pressure oscillations. The last of these phenomena is treated separately in Section 9.4.

The seismic loads experienced by the manifold structure are provided in Table A9.1.3-1. These loads are imposed as accelerations to the region being evaluated, consistent with the directions noted in the table.

The waterhammer pressure loads as they pertain to the manifold structure are made up of three components. The first of the components is an acoustic pressure wave, generated either outside of the steam generator due to valves opening or closing in the main feedwater line, or inside the steam generator due to steam bubble collapse. The second component of the waterhammer pressure load is due to flow loss as the flow passes through the perforated plates of the manifold. The third component of the pressure load is the momentum load imposed on various manifold components resulting from turning of the flow as it passes through the manifold.

The source of the acoustic waterhammer pressure loads is discussed in Section 8.0. The flow loss and momentum loads are both a function of the fluid velocity as it passes through the manifold. The fluid velocities for each of the waterhammer transients are also discussed in Section 8.0 together with the method used to determine the flow loss and momentum loads.

The acoustic pressure loads [illegible] function of time in the form of a decaying sine wave. The fluid velocities vary in a similar fashion with the oscillatory flow (flow overshoot) varying about a mean velocity. The approach taken in evaluating the time-varying pressure waves is to treat the peak pressures using a dynamic load factor approach. The peak pressure loads are applied to the structure statically with appropriate scaling of loads to account for dynamic effects. Using a modal analysis, the dominant natural frequencies are established for a given component. The natural period of the structure is then compared to the period of loading and a dynamic load factor is established. Any areas requiring dynamic load factors will be identified in the detailed analysis sections.

A summary of the waterhammer transients and the number of times each transient is postulated to occur in forty years is given in Table A9.1.3-2. Note that several transients are listed twice with different numbers of occurrences. The transients with a lower frequency of occurence are a result of balance of plant events having a much lower probability of occurrence, but which result in higher loads. The peak pressure loads, without dynamic load factors, for each of the waterhammer transients are contained in Tables A9.1.3-3 through A9.1.3-12.

The bubble collapse waterhammer loads for the manifold have been determined by test. The applicable pressure loads for the manifold are [ ]a,c,e for Upset and Faulted conditions, respectively.

A comparison of the three faulted loads; feedline break/check valve slam, safe shutdown earthquake, and faulted bubble collapse, shows the total load imposed on the manifold to be [.]a,c,e

A9.1.3.2 Thermal Conditions

The Steady State and Transient Thermal Conditions imposed on the manifold are in general the result of system operation which can produce variations in the temperature and flow rate of the feedwater flow. The structural response to these conditions is directly related to the time rate of change of the fluid, the overall change in fluid temperature, the fluid flow rate, and the film coefficient between the metal and water. Characteristics of the metal such as material density, specific heat, and thermal conductivity also affect the resulting structural response.

Section 8.0 provides a summary of the system thermal transients which affect the manifold. This summary includes a description of each transient, the time varying temperature and flow rate at the steam generator main feedwater nozzle, and the postulated number of occurrences. The list of transients which result in a change of the main feedwater temperature can be reduced to a set of seven umbrella events. The umbrellaing procedure used is discussed in more detail in the Thermal Hydraulics Section, Section 8.1. The seventh transient, excess bypass feedwater, results in a temperature variation in the downcomer. As a result, this transient does not affect the manifold box assembly, but rather affects the attachment welds for the manifold and flow splitter. The seven umbrella transients are shown in Table A9.1.3-13 with the number of cycles used in the fatigue calculations.

In addition to the time-varying temperature and flow-rate curves at the main feedwater nozzle, similar input was provided for the downcomer annulus through an analysis of the overall steam generator. The applicable boundary conditions are again contained in Section 8.3.

Apart from the rapid time-varying transients discussed above, there is a low flow rate (2 percent of nominal) condition which results in thermal stresses in the main feedwater nozzle region of the steam generator and also in the modification. The system event is forward flushing, and is intended to flush cold water from the main feedwater line at a low flow rate to preclude the initiation of bubble collapse pressure loads in the steam generator preheater region. The presence of the cold water in the main feedwater line is the result of events, such as reactor trip, which isolate the main feedwater nozzle for various periods of time. During these periods of isolation, the water temperature in the main feedwater line will decrease. In some situations the water will cool to ambient temperatures, which are assumed to be as low as 32°F.

During the forward flushing procedure the low flow rate allows water to stratify as it passes through the main feedwater nozzle region. This stratification results in a layer of cold water on the bottom of the feedwater nozzle with a layer of hot water above it. The transition zone between the hot and cold layers occurs over a small distance resulting in a rather sharp thermal interface. The temperature of the cold water will vary depending on downtime. The temperature distributions for this event applicable to the manifold were determined by test. The results of these tests are presented in Section 8.3. The applicable number of cycles for each of the stratification events is defined in Table A9.1.3-14 together with the applicable cold water temperatures.

A further consequence of forward flushing is that a condition known as "thermal striping" occurs at the interface of the hot and cold layers of water. Thermal striping is a high frequency oscillation of temperature at the surface of a metal. Thermal striping often occurs in regions where mixing of hot and cold fluids is occurring. Thermocouples placed at the fluid hot/cold interface in the flow stratification tests have verified that thermal striping is occurring. The thermal striping analysis is one of the several "comprehensive structural considerations" discussed in detail in Section 9.4.

TABLE A9.1.3-1

SUMMARY OF SEISMIC LOADS FOR MANIFOLD

SEISMIC DIRECTION*	ACCELERATION (g's) OBE	SSE
X - Direction	4.65	5.36
Y - Direction	4.54	5.24
Z - Direction	3.6	4.1

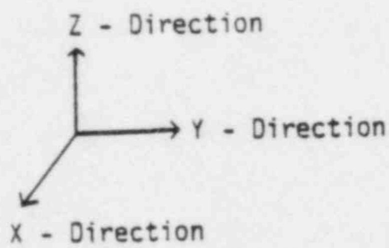

* Y - Direction is parallel to axis of steam generator main feedwater nozzle

TABLE A9.1.3-2

SUMMARY OF WATERHAMMER PRESSURE TRANSIENTS

TRANSIENT	NUMBER OF CYCLES
Switchover - With Bypass Flow	2,243 (1),(2)
Switchover - Without Bypass Flow	132 (2)
Feedwater Isolation From 100% Flow - A	765 (2)
Feedwater Isolation From 100% Flow - B	5 (2)
Excessive Feedwater - A	29
Excessive Feedwater - B	1
Check Valve Closure	10
Feedline Break/Check Valve Closure	1
Upset Bubble Collapse	10
Faulted Bubble Collapse	1

(1) This includes 1,570 cycles for a Plant Loading for Generic Plants, and 30 cycles for Excessive Feedwater Valve Opening.

(2) The total number of cycles for these events is consistent with Section 8.0, allowing for 30 cycles for Excessive Feedwater Valve Opening. Differences in number of cycles for specific events will not affect manifold fatigue usages.

Addendum
1-14-83.

TABLE A9.1.3-3

SUMMARY OF WATER HAMMER PRESSURE LOADS (1)

NORMAL OPERATING CONDITIONS

a,c,e

TABLE A9.1.3-4

SUMMARY OF WATER HAMMER PRESSURE LOADS (1)

SWITCHOVER - WITH BYPASS FLOW

a,c,e

TABLE A9.1.3-5

SUMMARY OF WATER HAMMER PRESSURE LOADS (1)

SWITCHOVER/WITHOUT BYPASS FLOW

LOADED SURFACE	ΔP - ACOUSTIC	ΔP - FLOW LOSS	ΔP - MOMENTUM	ΔP - TOTAL

a,c,e

TABLE A9.1.3-6

SUMMARY OF WATER HAMMER PRESSURE LOADS (1)

FEEDWATER ISOLATION FROM 100% FLOW-A

a,c,e

TABLE A9.1.3-7

SUMMARY OF WATER HAMMER PRESSURE LOADS (1)

FEEDWATER ISOLATION FROM 100% FLOW-B

LOADED SURFACE	ΔP - ACOUSTIC	ΔP - FLOW LOSS	ΔP - MOMENTUM	ΔP - TOTAL

a,c,e

TABLE A9.1.3-8

SUMMARY OF WATER HAMMER PRESSURE LOADS (1)

EXCESSIVE FEEDWATER-A

LOADED SURFACE	ΔP - ACOUSTIC	ΔP - FLOW LOSS	ΔP - MOMENTUM	ΔP TOTAL

a,c,e

TABLE A9.1.3-9

SUMMARY OF WATER HAMMER PRESSURE LOADS (1)

EXCESSIVE FEEDWATER-B

a,c,e

LOADED SURFACE	ΔP - ACOUSTIC	ΔP - FLOW LOSS	ΔP - MOMENTUM	ΔP - TOTAL

TABLE A9.1.3-10

SUMMARY OF WATER HAMMER PRESSURE LOADS (1)

CHECK VALVE CLOSURE

LOADED SURFACE	ΔP - ACOUSTIC	ΔP - FLOW LOSS	ΔP - MOMENTUM	ΔP - TOTAL

a,c,e

TABLE A9.1.3-11

SUMMARY OF WATER HAMMER PRESSURE LOADS [(1)]

FEEDLINE BREAK/CHECK VALVE CLOSURE

FLOW OUT STEAM GENERATOR (BLOWDOWN)

LOADED SURFACE	ΔP - ACOUSTIC	ΔP - FLOW LOSS	ΔP - MOMENTUM	ΔP - TOTAL

a,c,e

TABLE A9.1.3-12

SUMMARY OF WATER HAMMER PRESSURE LOADS (1)

FEEDLINE BREAK/CHECK VALVE CLOSURE

FLOW INTO STEAM GENERATOR (CHECK VALVE SLAM)

LOADED SURFACE	ΔP - ACOUSTIC	ΔP - FLOW LOSS	ΔP - MOMENTUM	ΔP - TOTAL

a,c,e

TABLE A9.1.3-13

SUMMARY OF SEVEN UMBRELLA TRANSIENTS

TRANSIENT	CYCLES(1)
PLANT LOADING	13,200
REACTOR TRIP WITH COOLDOWN & S. I.	30
LARGE STEP LOAD DECREASE	670
TWO BANKS OF HEATERS OUT OF SERVICE	360
EXCESS FEEDWATER	30
PLANT UNLOADING	12,200
EXCESS BYPASS FLOW	40

(1) CORRESPONDS TO TOTAL NUMBER OF CYCLES OF UMBRELLAED TRANSIENTS

TABLE A9.1.3-14

NUMBER OF FORWARD FLUSHING TRANSIENTS

TRANSIENT	MINIMUM FEEDWATER TEMPERATURE - °F						Total	COMMENTS
	32	100	150	160	200	>250		
Large Step Decrease	--	--	--	200	--	--	200	
Loop Out of Service	50	--	--	--	--	--	50	A maximum of 50 transients of the total 70 N-1 transients conservatively assumed to occur in one loop.
Plant Loading (0% to 100%)	188	63	63	--	63	123	500	
Upset Transients	120	40	40	--	160	440	800	
Plant Unloading (100% to 0%)	--	--	--	--	--	500	500	Procedure modification will prevent final temperature of less than 280°F
TOTAL (For worst one loop)	358	103	103	200	223	1063	2050	
							2070	Total All Loops

NOTES: Based upon typical "bad" plant
Conservatively used 280°F for upset and plant loading transients instead of 440°F
Assumed ambient temperature of 32°F

A9.1.4 Structural Criteria

Primarily, the ASME Boiler and Pressure Vessel Code, Section III, Subsections NB and NG are used to evaluate the manifold configuration for normal/upset loads, and Section III, Appendix F is used for faulted loads. This criteria is specified as a guide to evaluate the manifold. Any deviation from the code criteria is noted explicitly in the appropriate evaluation section. For faulted loads, the ultimate criteria for the manifold is that it not prevent the primary boundary from maintaining its structural integrity throughout the duration of any faulted event.

A summary of the structural materials is given in Table A9.1.2-1. The allowable stresses for normal/upset and faulted loading conditions based on the above criteria is summarized in Table A9.1.4-1. The acceptable fatigue usage is 1.0.

TABLE A9.1.4-1

SUMMARY OF ALLOWABLE STRESSES(1), (2)

Material	Design/Normal/Upset		Faulted		
	S_m	$P_L + P_b + Q$	S_m	P_m	$P_L + P_b$

a,c,e

A9.1.5 Analysis Overview

The analysis of the internal manifold discussed in the following sections represents an integrated analysis involving two box-interaction analyses and several detailed analyses. A flow chart detailing the flow of information between the various analyses is shown in Figure A9.1.5-1.

The initial step in the analysis process is the development of shell models for the top, middle, and bottom boxes located on the left of the manifold centerline. This is indicated at the far left of the analysis flow chart. Once the models have been generated, a substructure which contains the prescribed structural loads is developed for each box (Phase I). Having generated the substructures, the box-to-box interaction analysis is then performed in Phase II. The results of Phase II are then used to develop detailed stresses and displacements for each of the individual boxes (Phase III). The results of Phase III are then used to provide boundary condition input for the detailed structural models which consider only a local portion of the overall manifold.

Two interaction analyses are performed following this process and leading to the final detailed evaluations. The first considers the mechanical load conditions. The second interaction analysis considers the thermal events imposed on the manifold. The flow of information in the second analysis is the same as for the mechanical loads, except that a heat transfer analysis is required for each box for each transient, prior to Phase I.

FIGURE A9.1.5-1

MANIFOLD ANALYSIS FLOW CHART

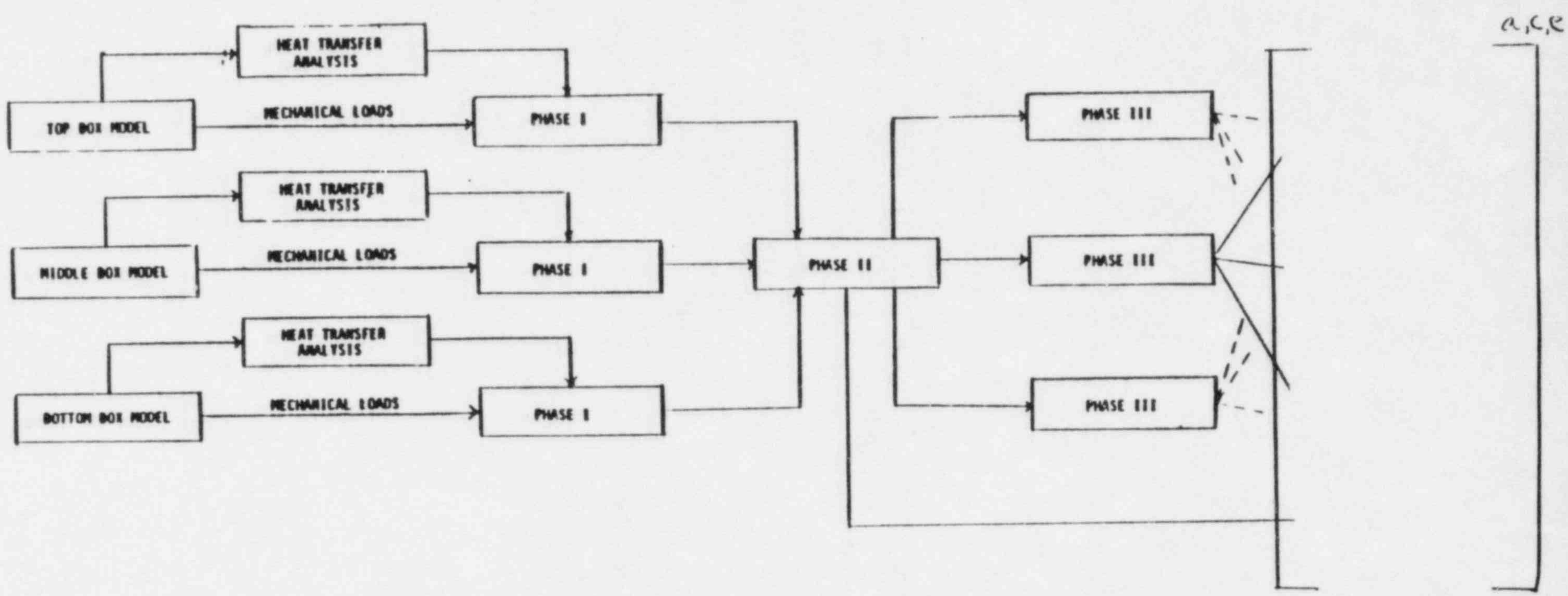

A9.1.6 Manifold Box Interaction/Primary Load Evaluation

A9.1.6.1 Introduction

The manifold box interaction analyses for primary load evaluation provide general structural behavior of the manifold due to pressure transient loadings and seismic loads; natural frequency determination; stress evaluation of areas not included in the local finite element models; and boundary conditions for local model analyses.

The finite element method of analysis was used for primary load evaluation of the manifold structure. Figures A9.1.6-1 and A9.1.6-2 illustrate the finite element representation of the six box manifold structure. Individual box finite element representations are shown in Figures A9.1.6-3 thru A9.1.6-5. A half-symmetry, three left-hand box manifold model is given in Figures A9.1.6-6 and A9.1.6-7.

A9.1.6.2 Summary of Results

From the manifold box interaction analyses, the maximum stress intensity results for each of the manifold box plates for normal/upset pressure transients and OBE are given in Table A9.1.6-1 for membrane stress intensity and in Table A9.1.6-2 for membrane plus bending stress intensity. For faulted pressure transients and SSE, membrane and membrane plus bending stress intensities and maximum strains are shown in Table A9.1.6-3 and Table A9.1.6-4, respectively. The manifold structure has been evaluated by elastic and elastic-plastic analysis for faulted pressure conditions. The elastic-plastic dynamic analysis is presented in Section A9.1.6.6. The stud and bolt loads for the pressure transients are given in Table A9.1.6-5.

Natural frequencies for the manifold box structure are listed in Table A9.1.6-6, and shown graphically in Figure A9.1.6-8 through A9.1.6-10.

A9.1.6.3 Manifold Structure Overview

The total manifold structure was modeled for finite element analysis (Figure A9.1.6-1). The basic structure consists of six individual boxes bolted together by 24 threaded fasteners and welded to a cylindrical flange. The flange is then welded to the thermal liner. The overall structure is symmetric about its vertical and horizontal centerlines. Figure A9.1.6-2 shows the six boxes with the continuous flange sectioned for illustration purposes. For identification, the six boxes plus flange sections are designated as left-hand or right hand boxes and as top, center or bottom boxes. A 0.060 inch gap exists between boxes as indicated in Figure A9.1.6-3.

Each individual box consists of component plates which are as follows:

a,c,e

The plates are identified for the top left-hand box in Figure A9.1.6-4 and the web plates and flange divisions are shown in Figure A9.1.6-5 for the center left-hand box. Bolt and tapered stud locations are indicated in both figures.

A9.1.6.4 Analysis Procedure

For the manifold box interaction analyses, the WECAN general purpose finite element analysis computer code (Reference (A9.1-1) and its superelement analysis technique were used. In general, the superelement analysis technique consists of three phases of analysis plus post-processing for stress and displacement solutions.

Phase 1 involves the generation of component structures as STIF60 superelements. These components are the six boxes with corresponding flange sections (Figure A9.1.6-2). For each box, a Phase 1 run generates a stiffness matrix, mass matrix and load vectors in terms of a reduced set of degrees of freedom (DOF's) for that box. The set of DOF's for a box are specified in Phase 1 and consists of potential contact or bolt connection DOF's with other boxes, flange continuity points, structural constraint points or mass DOF's for natural frequency determination (modal analysis). Load vectors, depending on the type of analysis, include unit pressure loads on individual plates or unit accelerations due to gravity in the X, Y, or Z direction.

For a superelement box, the individual plates were modeled using the STIF24 flat shell element. Material properties for the exit plate and entrance plate were modified according to Reference (A9.1-5) to account for perforation. For the modal analysis, material properties were also revised to include the effect of hydrodynamic mass (References (A9.1-4) and (A9.1-6)).

The Phase 2 portion of the superelement analysis technique determines the overall manifold structural response using the individual box superelements in conjunction with structural constraints, contact gaps/hooks (pretensioned bolts) between boxes and/or direct connection of boxes. In this phase, the load vectors from Phase 1 were factored and combined when applied to their corresponding superelements and cylindrical flange continuity was established. Contact gaps and pretensioned bolts, when used, were STIF40 one-dimensional dynamic gap elements. Results from Phase 2 include bolt and stud loads and displacement solutions for each substructure. For modal analysis, natural frequencies are also obtained.

Phase 3 applies to a particular superelement box, the displacement solution for the reduced set of DOF's from Phase 2 and using the corresponding combination of load vectors, determines the stress distribution and displacement solution for the plate elements of that box.

Post-processing of Phase 3 results for a given loading includes box displacement plots and stress contour plots of plates Reference (A9.1-7). Since the exit and entrance plates are perforated and the modified material properties provided mean stress results, component stress results required stress factors for peak stress determination (Reference (A9.1-5)). Peak stresses from the overall manifold analysis were used only for comparison with local finite element model results.

A9.1.6.5 Analysis Models and Loadings

Three mechanical load condition box interaction analyses were performed on the manifold structure. Because of vertical centerline symmetry of the loadings and structure, a three-box, left-hand symmetry model was used to analyze the manifold for the pressure transients plus dead weight loadings. For the seismic and modal analyses, all six boxes of the manifold were required because of the asymmetric aspect of the loading and the vertical-centerline box nonlinearity. Modeling characteristics and loading for the three analyses are summarized below.

The ten pressure transient load cases are given in Tables A9.1.3-3 through A9.1.3-12. The three left-hand box models shown in Figures A9.1.6-6 and A9.1.6-7 were used to model the manifold. Phase 1 runs for each box had unit pressure load vectors for the individual plates and dead weight for the structure. In Phase 2, the unit plate pressure load vectors and dead weight were factored and combined for each of the ten pressure cases. The Phase 2 model had preloaded studs and bolts, vertical contact gaps between horizontal box surfaces, vertical-centerline-symmetry, horizontal contact gaps to ground, flange continuity between boxes, constraint to ground and flange symmetry boundary conditions at the vertical-symmetry centerline. Bolt preload was [ ]a,c,e

Bolt and stud preload can vary between [ ]a,c,e These variations are accounted for when required in the threaded fastener evaluation, Section A9.1.11.

The manifold model was analyzed for the normal/upset pressure transients of excessive feedwater-B and check valve closure, and for the two faulted feedline break/check valve closure pressure transients using the configuration employing tapered studs and the[ ]a,c,e gap. All vertical bolts and tapered studs were given shear transfer capabilities. All other cases were analyzed with no gap and with no shear transfer capability in the vertical fasteners. These cases also had one less fastener, the outer most, radially from the nozzle centerline, reflecting the original manifold design.

Seismic loads consisted of factored static accelerations due to gravity loadings for OBE and SSE. Table A9.1.3-1 summarizes the load factors. For these load cases, a six box model (Figure A9.1.6-2) was used. Phase 1 models had load vectors consisting of unit accelerations due to gravity in the X, Y and Z directions. Contact DOF's on the boxes due to pretensioning of bolts and general potential contact of boxes were specified in Phase 1. The Phase 2 model included bolt preload[ ]a,c,e and vertical (top-bottom plates) and horizontal (centerline end plates) contact gaps between boxes.

The modal analysis for natural frequency determination also consisted of six superelement boxes (Figure A9.1.6-2). Structural and hydrodynamic mass and direct box interconnection DOF's for each box were specified in Phase 1. Three different Phase 2 model configuration cases were analysed due to the nonlinearity of the manifold structure and the linear aspect of modal analysis. The three cases were: [

]a,c,e Depending on the frequency and mode of interest, a second or third case result provides the best representation of the structural dynamic characterization of the manifold.

A9.1.6.6 Manifold Faulted Analysis - Feedline Break/Check Valve Slam (FLB/CVS)

The manifold assembly was initially analyzed elastically for the faulted FLB/CVS as an equivalent static condition. The stress results indicate that most of the structure satisfies the primary stress limits of Appendix F of the ASME Code, Section III, using elastic analysis. These results are presented in Tables A9.1.6-3 and A9.1.6-4 and in Sections A9.1.8 and A9.2.1. In addition, it has been shown with the assumption of a failed liner/manifold weld, that the tubing can withstand the impact of the manifold assembly driven by the FLB/CVS, Section 9.4.4. In Tables A9.1.6-3 and A9.1.6-4, regions designated by the footnotes (1) and (2), are shown in Figure A9.1.6-11. These regions would achieve stress levels that indicate the necessity for further evaluation.

The basic requirement for the evaluation of the manifold assembly for the FLB/CVS is to assure the integrity of the primary, pressure retaining boundary, i.e., the tubing (see Section 9.4.4). Appendix F of the ASME Code, Section III, is a non-mandatory criteria that may be used to demonstrate integrity of the involved structures. Primary membrane and primary membrane plus bending stress limits are prescribed in the Code. Thermal stresses and other secondary stresses need not be considered since they are displacement controlled and the forces are not required to be sustained to maintain equilibrium. The manifold assembly structure can be represented structurally as shown in Figure A9.1.6-12 for the net loading applied during the FLB/CVS. For either case, the bending in the flanges is secondary since moments are not required for equilibrium. For flow out, the midplane of symmetry is in compression, the bolts are not loaded, and the stresses are acceptable throughout on an elastic basis. For flow in, the bolts are not required since the wrapper provides reaction support to the applied loads and is a limit device for manifold displacement. In each case, the axial reaction force at the manifold to liner weld is primary. It has been shown by elastic analysis in Section A9.1.8 that the primary stress limits are satisfied for this weld. The regions designated by the footnotes (1) and (2) in Table A9.1.6-3 and A9.1.6-4 and in Figure A9.1.6-11 are therefore regions of secondary stress and it is not mandatory for them to satisfy primary stress limits. However, an elastic-plastic dynamic analysis was performed in a simplified manner to demonstrate that the manifold structure is capable of absorbing the energy applied during the FLB/CVS without failure.

This was accomplished by making use of the elastic dynamic analysis results, the peak, equivalent static forces of the top box, and the stress-strain properties of the bolt and manifold plate materials. Stress levels from the elastic analysis were reviewed to determine that the most highly loaded bolt would yield before the box. [

]a,c,e

[

]a,c,e

The evaluation of the manifold assembly for the postulated FLB/CVS faulted event demonstrates the following:

1) The primary stresses in required locations satisfy the elastic primary limits of Appendix F of the ASME code, Section III.

2) The secondary strains in critical sections will not exceed the allowable material elongation at temperature.

3) The additional assumption of a failed manifold/liner weld will not result in loss of integrity of the tubing primary boundary.

a,c,e

Table 9.1.6-1 to 9.1.6-6 showing stress intensities of transient and Figure 9.1.6-1 to 9.1.6-7 showing finite element models of design modification are considered Westinghouse Proprietary.

a,c,e

THESE FIGURES ARE CONSIDERED PROPRIETARY
IN THERE ENTIRITY

FIGURES 9.1.6-8 TO 9.1.6-10
MODE SHAPES AND NATURAL FREQUENCEIES
CASE 1, CASE 2, CASE 3

a,c,e

FIGURE A9.1.6-11 AREAS OF MAXIMUM MEMBRANE PLUS BENDING STRESS INTENSITIES - FAULTED PRESSURE TRANSIENT

a,c,e

FIGURE A9.1.6-12 **MANIFOLD ASSEMBLY STRUCTURAL REPRESENTATION DURING FLB/CVS**

A9.1.7 Manifold Interaction/Thermal Transient Analysis

A9.1.7.1 Introduction

This section investigates the general effects of thermally induced displacements and stresses on the manifold and the interaction of the manifold boxes. This analysis was performed using the WECAN computer code. The results of this analysis were used as input for the finer mesh models and as confirmation that the critical regions were properly identified for further study. The loads transmitted through the bolts [ ]a,c,e were also obtained in this process.

A9.1.7.2 Analysis Method

The analysis was performed using a similar WECAN computer model as generated for the primary load evaluation. Figure A9.1.6-7 contains a computer generated plot of the model. The analysis was performed in two steps. The metal temperature solutions as a function of time were obtained in the first step. The critical times in the transient were identified by plotting ΔT's between adjacent metal points. The critical times selected by this process were later confirmed with the fine mesh models of the critical regions.

The selected metal temperatures were then used in the second step of the analysis to obtain the stress and displacement solutions. The size of the model required that this step be accomplished by using the same super element technique as was used in the Primary Load Evaluation Sections. This technique is discussed in detail in Section A9.1.6.4. The displacements and metal temperatures were then made available to the finer mesh model, where the detailed ASME Code evaluations were performed.

A9.1.7.3 Loadings Considered

The analysis investigates the thermal transients as discussed in Section 8.0 of this design report. The unit is exposed to many different types of thermal conditions and this analysis will address each of the conditions. However, some of the thermal transients can be conservatively grouped together due to the similar boundary conditions the transients impose on the structure. This was done to reduce the total number of computer runs required to determine the response of the manifold assembly. Section A9.1.3.2 contains a summary of the thermal transients investigated in this analysis. Note that this analysis investigates the effects of feedwater stratification due to forward flushing. Three flow rates were investigated (2.35 percent, 2.00 percent and 1.50 percent of full flow).

A9.1.7.4 Summary of Results

The purpose of this analysis was to obtain the temperature and displacement boundary conditions for use in the fine mesh models and to obtain the interaction loads being transmitted through the bolts. The temperature and displacement boundary conditions were used in the fine mesh models to determine the detailed stress solutions. ASME Code evaluations were performed using the results of the fine mesh models.

The analysis determined the magnitude of the loads being transmitted through the bolts due to the interaction of the boxes. The threaded fasteners were evaluated and the results are contained in Section A9.1.11 of this document. The axial bolt loads, moments, rotations and gap contact forces that were used in the fastener evaluation are contained in Tables A9.1.7-1 thru A9.1.7-13. Table A9.1.7-3 and Table A9.1.7-4 also contain the [

.]^{a,c,e} Tables A9.1.7-14 thru Table A9.1.7-15 contain the inplane shear forces at the bolt locations.

a,c,e

THESE TABLES ARE CONSIDERED PROPRIETARY

IN THERE ENTIRITY

TABLE 9.1.7-1 TO 9.1.7-4
THERMAL LOADS

TABLE 9.1.7-5 TO 9.1.7-12
BENDING MOMENTS IN BEAM AT
VARIOUS NODES.

TABLE 9.1.7-13 TO 9.1.7-15
OUT-OF-PLANE ROTATIONS AND
IN-PLANE NODAL FORCES.

A9.1.8 Manifold Flange/Thermal Liner Weld Analysis

A9.1.8.1 Introduction

This section discusses the evaluation of the welds connecting the manifold assembly to the thermal liner. These welds are located where the flange segments from each of the manifold boxes are welded to the sleeve, at the center of the sleeve where the inconel and carbon steel sections are joined, and at the fillet weld between the sleeve and the thermal liner.

In addition to the manifold attachment welds, the effect on the thermal liner to wrapper weld is considered.

The sections to follow present the conclusions based on the results of the evaluations, and a detailed description of the supporting mechanical and thermal analyses and the ASME Code evaluations for Faulted and Normal and Upset conditions.

A9.1.8.2 Conclusions

The manifold flange, the flange/sleeve weld, the sleeve bi-metallic weld, the sleeve/liner weld and the liner/wrapper weld meet the Code allowables for Faulted, Normal and Upset conditions. This region of the manifold assembly and the existing structure to which it is attached therefore satisfy design requirements.

A9.1.8.3 Summary of Results

The manifold flange and associated attachment welds were evaluated for Faulted, Normal and Upset conditions. The results of the Faulted evaluation are summarized in Table A9.1.8-1. The calculated stress intensities for all sections evaluated are less than the Code allowables. The results of the maximum range of stress intensity and fatigue evaluations are summarized in Table A9.1.8-2. The Code allowables are satisfied for Normal and Upset conditions for all locations.

A9.1.8.4 Material Properties

The materials for each of the components included in this analysis are listed in Table A9.1.8-3. Temperature dependent material properties were used for all heat conduction and stress analyses performed for this evaluation. The values used for each of the properties are contained in section A9.1.2.

Table A9.1.8-3

a,c,e

Component	Material

A9.1.8.5 Summary of Loading Conditions

The loading conditions applied to the manifold assembly are discussed in detail in section A9.1.3. This section summarizes the loads applied to different regions of the structure considered in this analysis. The waterhammer pressure transients are those identified in Table A9.1.3-2. The pressures applied to the manifold flange area were taken from Tables A9.1.3-3 to A9.1.3-12 and are given in Table A9.1.8-4.

The six umbrella thermal transients shown in Table A9.1.3-13 and the forward flushing events defined in Table A9.1.3-14 make up the set of thermal events to be applied to the manifold flange area.

A9.1.8.6 Finite Element Model

In order to evaluate the manifold to liner attachment welds, it was necessary to include part of the manifold in the finite element model. This was particularly important for transferring net pressure loads to the flange. Figure A9.1.8-1 indicates the parts of the back plates of each of the manifold boxes included in the finite element model for this evaluation.

The finite element model used for this analysis is shown in Figure A9.1.8-2. Included in this model are the parts of the back plates shown on the previous figure, the manifold flange, the bimetallic sleeve and the welds attaching it to the flange and the thermal liner, part of the liner with sufficient length to attenuate end effects, and the thick part of the wrapper attached to the thermal liner. Two features of this model not apparent on this figure are that the manifold segments are independent of each other up to the weld with the sleeve, and that the backing strip is included in the model such that it is not attached to the flange.

This model is formed from WECAN (Reference (A9.1-1)) 3-D isoparametric elements STIF48 and STIF55 for the stress analysis and the companion elements STIF49 and STIF65 for the thermal analysis. A total of 702 elements were used to form the model.

Figure A9.1.8-3 shows the displacement boundary conditions used for the pressure cases. The shaded part of the model on the plane of symmetry indicates where the symmetry conditions were applied. [

]a,c,e Along the shaded edges of the back plate segments displacements obtained from the results of the manifold box interaction analysis were applied in order to properly transfer the net pressure loads to the flange from the rest of the manifold assembly. Pressures are also applied to the appropriate surfaces of the back plates, flange and wrapper to represent any pressure drops acting across those surfaces.

[ ]a,c,e

[ ]a,c,e

The thermal boundary conditions (fluid temperature, effective film coefficients) are consistent with those used for the thermal analysis of the manifold assembly in section A9.1.7.2, with additional data for the liner and wrapper taken from Section 8.0.

The boundary conditions for the thermal stress analysis are shown on Figure A9.1.8-4. The displacement constraints on the plane of symmetry, the end of the liner and the edge of the wrapper are identical to those used for the pressure cases.

[ ]a,c,e

A9.1.8.7 Heat Transfer Results

The six umbrella thermal transients were run on WECAN using the transient heat conduction solution option. [

]a,c,e

Representative results for one of the transients are shown on Figures A9.1.8-5 to A9.1.8-8. The first of these plots shows the temperature variations during the large step load decrease transient on a section through the sleeve and liner at the weld joining those components. Curve 1 is the temperature on the inside surface of the sleeve, while curve 9 is the temperature of the outside surface of the liner. Figure A9.1.8-6 shows the temperature differences of selected nodes at the same section. Curve 1 is the difference in temperature between the surface node and its adjacent node on the section. Curve 2 is the ΔT between the surface and the middle of the sleeve, and curve 3 is the ΔT between the middle of the sleeve and the middle of the liner. Peaks in curves 1 and 2 indicate the times of maximum stresses while peaks in curve 3 indicate the times of [

] a,c,e For this transient the peaks for both types of stress occur at [ ] a,c,e Figure A9.1.8-7 and A9.1.8-8 are the same type of plots for a section through the flange/sleeve weld and also identify [ ] a,c,e as the critical time for stress evaluation.

The times selected for the remaining umbrella transients were chosen in the same manner. They are identified in Table A9.1.8-5.

A9.1.8.8 Stress Results

Figures A9.1.8-9 through A9.1.8-18 contain contour plots of displacements, temperatures, and stress intensities on different sections through the model for three representative load conditions. Figures A9.1.8-9 to A9.1.8-11 show the displacements, temperatures and stress intensities occurring at 60 seconds into the large step load decrease transient on two sections through the model. The top half of each of these figures plots the above quantities on a section at the symmetry plane in the top part of the model. The bottom half of each figure plots the same quantities on a section through the top manifold box where it meets the middle box.

Figures A9.1.8-12 to A9.1.8-15 present some sample results for the thermal stratification case at 2.2 percent flow. Figure A9.1.8-12 shows the displacements and temperature distribution in the manifold back plates. Figure A9.1.8-13 gives the circumferential temperature distributions on sections through the flange/sleeve and sleeve/liner welds. The next two figures show the variation in stress intensity patterns and magnitudes for sections on the plane of symmetry and at the bottom edges of the top and middle manifold boxes.

Figures A9.1.8-16 to A9.1.8-18 present results for the check valve closure pressure case. For this and the other pressure cases, displacements obtained from the results of the manifold assembly interaction analysis were applied to the edges of the back plate. Figure A9.1.8-16 clearly shows the effect of these boundary conditions[ ]a,c,e The next two figures show the displacement and stress intensity variations for sections on the vertical and horizontal edges of the top manifold box.

A9.1.8.9 Evaluation for Faulted Conditions

The faulted conditions with the largest pressure drops at the feedwater nozzle are feedline break with check valve closure and bubble collapse waterhammer. Stresses were determined for the feedline break condition for flow both out of and into the preheater region. Bubble collapse was not analyzed explicitly, but stresses for the pressure pulse of[ ]a,c,e can be obtained by scaling the stresses obtained for the check valve closure event by the ratio of the acoustic ΔP's across the back plates and flange for the two events. The resulting scale factor is[ ]a,c,e The faulted conditions considered for this evaluation are listed in Table A9.1.8-6.

The faulted evaluations (as well as those for Normal and Upset conditions in the next section) were performed with the automated ASME Code evaluation program, WECEVAL (Reference (A9.1-8)). WECEVAL performs the Code evaluations for lines of nodes through the thickness, called analysis sections. The analysis sections selected for this evaluation are shown on Figure A9.1.8-19. On this figure a series of analysis sections is indicated for each location. That represents an analysis section every 15° around the circumference with the first number being the section at the top of the model and the last number the section at the bottom. The separate flange segments have an additional two analysis sections in order to evaluate the segments on each side of the planes between the manifold boxes.

Many of these analysis sections are located at welds and must have their primary stress limits adjusted by a weld quality factor and must incorporate a fatigue strength reduction factor in their fatigue evaluation. Table A9.1.8-7 summarizes the information taken from Table NG-3352-1 of Reference (A9.1-3) for each set of analysis sections.

According to Appendix F of the ASME Code, the primary stress limits are the lesser of $2.4S_m$ or $0.7S_u$. The allowable stress intensities for faulted events at 440°F (feedline break) and 550°F (bubble collapse) are summarized in Table A9.1.8-8 for each set of analysis sections.

The results of the faulted evaluations are presented in Table A9.1.8-9. This table contains the maximum value of the ratio of the calculated stress intensity to the allowable stress for each set of analysis sections. All such ratios are less than one. Therefore the manifold flange and its attachment welds satisfy Code allowables for Faulted conditions.

A9.1.8-10 Evaluation for Normal and Upset Conditions

The Normal and Upset load conditions which were considered for the maximum range of stress intensity and fatigue evaluations were taken from Tables A9.1.3-2, and A9.1.3-13. These load conditions are identified in Table A9.1.8-10. Scale factors on thermal stresses for some of these load conditions were determined by dividing the actual ΔT by the ΔT at the time thermal stresses were calculated.

WECEVAL requires values for S_m and E_{curve}/E_{actual} to carry out the maximum range of stress intensity and fatigue evaluations. These are given in Table A9.1.8-11.

The results of the evaluations for Normal and Upset conditions are summarized in Table A9.1.8-12. The stress ratios or fatigue usage factors listed in this table are the maximum values calculated for each set of analysis sections.

TABLE 9.1.8-1

RESULTS OF FAULTED EVALUATION

SECTION	MAXIMUM STRESS INTENSITY/ ALLOWABLE

a,c,e

(1) EVALUATION PERFORMED OVER FULL CROSS-SECTION

(2) P_L

(3) $P_m + P_b$

(4) P_m

TABLE 9.1.8-2

RESULTS OF NORMAL AND UPSET EVALUATION

SECTION	MAXIMUM RANGE/ ALLOWABLE	FATIGUE USAGE FACTOR

a,c,e

Addendum
1-14-82

TABLE 9.1.8-4

PRESSURE LOADS

a,c,e

PRESSURE CASE	SURFACE ΔP's
NORMAL OPERATING	
SWITCHOVER (WITH BYPASS FLOW)	
SWITCHOVER (WITHOUT BYPASS FLOW)	
FEEDWATER ISOLATION FROM 100 PERCENT FLOW-A	
FEEDWATER ISOLATION FROM 100 PERCENT FLOW-B	
EXCESSIVE FEEDWATER-A	
EXCESSIVE FEEDWATER-B	
CHECK VALVE CLOSURE	
FEEDLINE BREAK/CHECK VALVE CLOSURE (IN)	
FEEDLINE BREAK/CHECK VALVE CLOSURE (OUT)	

TABLE 9.1.8-5

TIMES FOR THERMAL STRESS EVALUATION

TRANSIENT	TIMES (SEC)
PLANT LOADING	
REACTOR TRIP WITH COOLDOWN & S. I.	
LARGE STEP LOAD DECREASE	
TWO BANKS OF HEATERS OUT OF SERVICE	
EXCESS FEEDWATER	
PLANT UNLOADING	

a,c,e

a,c,e

TABLE 9.1.8-6

FAULTED CONDITIONS

CONDITION	UNIT PRESSURE LOAD	SCALE FACTOR
FEEDLINE BREAK - FLOW OUT OF PREHEATER	B-8 (OUT)	[
FEEDLINE BREAK - FLOW INTO PREHEATER	B-8 (IN)	
BUBBLE COLLAPSE (+ΔP)	B-7	
BUBBLE COLLAPSE (-ΔP)	B-7	] a,c,e

a,c,e

THESE TABLES ARE CONSIDERED PROPRIETARY

IN THERE ENTIRITY

TABLE 9.1.8-7

ANALYSIS SECTION CLASSIFICATIONS

TABLE 9.1.8-8

ALLOWABLE STRESS INTENSITIES FOR FAULTED EVENTS

TABLE 9.1.8-9

RESULTS OF FAULTED EVALUATION

a,c,e

THIS TABLE IS CONSIDERED PROPRIETARY IN ITS ENTIRITY

TABLE 9.1.8-10

NORMAL AND UPSET LOAD CONDITIONS

TABLE 9.1.8-11

Sm's AND MODULI CORRECTION FACTORS FOR NORMAL AND UPSET EVALUATIONS

ASNS	TEMPERATURE(1)	Sm(2)	E curve/E actual
1 - 15	440	23.3	.8713
21 - 35	440	23.3	.8713
41 - 53	440	22.38	1.0737
61 - 73	440	22.38	1.0737
81 - 93	440	21.22	1.1211
101 - 113	500	20.5	1.1364
121 - 133	500	16.2	1.1364
141 - 153	440	23.3	.8713
161 - 173	440	22.38	1.0737

(1) TEMPERATURE IS °F.

(2) Sm IS KSI.

TABLE 9.1.8-12

RESULTS OF NORMAL AND UPSET EVALUATIONS

a,c,e

Addendum
1-14-83

a,c,e

Figures 9.1.8-1 to 9.1.8-4 showing finite element models of design modification are considered Westinghouse Proprietary.

a,c,e

THESE FIGURES ARE CONSIDERED PROPRIETARY
IN THERE ENTIRITY

FIGURES 9.1.8-5 TO 9.1.8-8 TEMP. VARIATION PLOTS

FIGURES 9.1.8-9 TO 9.1.8-18 DISPLACEMENT AND STRESS PLOTS FOR THE MANIFOLD

a,c,e

THIS FIGURE IS CONSIDERED PROPRIETARY
IN ITS ENTIRITY

FIGURE 9.1.8-19: LOCATION OF ANALYSIS SECTIONS FOR CODE EVALUATION

A9.1.9 Back Plate/Entrance Plate/Exit Plate Juncture

A9.1.9.1 Introduction

This section presents the results of the back plate/entrance plate/exit plate juncture evaluation as well as the method of analysis of the juncture.

The analysis includes faulted evaluations, maximum range of stress intensity evaluations and fatigue evaluations for the mechanical and thermal load conditions defined in Section A9.1.3.

A9.1.9.2 Summary and Conclusions

It has been shown that for the mechanical and thermal loads imposed on the juncture, the welds in the entrance, exit and top/bottom plates, as well as the hole boundaries, satisfy the stress and fatigue limits of the ASME Code, Section III. Tables A9.1.9-1 and A9.1.9-2 provide the results of the stress evaluation and the fatigue usage factors obtained.

A9.1.9.3 Configuration

Figures A9.1.9-1 through A9.1.9-5 depict the details of the Steam Generator Model D2/D3 Internal Manifold with the back plate/entrance plate/exit plate juncture highlighted. Design dimensions of these figures were used to develop the finite element model for the analysis.

A9.1.9.4 Finite Element Model

The finite element model is formed from the 20-node version of the WECAN Three-Dimensional Isoparametric Solid Element, STIF 48/STIF 49, and 15- node version of the WECAN Three-Dimensional Isoparametric Wedge, STIF 55/ STIF 65. The general view of the finite element model is given in Figures A9.1.9-6 and A9.1.9-7. Figures A9.1.9-8 and A9.1.9-9 show the details of the finite element model. The present finite element model is a detailed model following the overall manifold finite element models. The darkened regions of the overall model (see Figure A9.1.9-10) depict the box parts used for development of the detailed finite element model. The total number of elements in the model is 672, the number of unique nodes is 5405.

[ ] a,c,e

A9.1.9.5 Materials

Below, the bill of material numbers of juncture components are given:

Component	Material Number
Entrance Plate	[ ] a,c,e
Exit Plate	
Back Plate	
Top Plate	
Bottom Plate	

[ ]a,c,e The entrance and exit plates are perforated plates with rhombic patterns of circular holes. For the analysis of perforated plates the concept of the equivalent solid plate was utilized. The main part of the entrance and exit plates were replaced by geometrically similar equivalent solid plates with modified, effective properties. In the detailed stress/strain evaluation of the welds, the regions of the entrance and exit plates located in the vicinity of the back plate were considered as solid material with holes.

For the entrance and exit plates, material identification is shown in Figure A9.1.9-11 and Figure A9.1.9-12. The material properties of Inconel 600 are given in Section A9.1.2. The effective elastic constants of perforated plates including the film coefficients, were calculated from the corresponding data for solid materials taking into account the plate porosities. In the cases of thermal transients and stress/strain calculations, all the material properties, elastic and thermal, were considered as temperature dependent.

A9.1.9.6 Heat Transfer Results

a,c,e

These sets represent the time and positional variations of the feedwater bulk temperatures and film coefficients for the thermal boundary conditions applied to the model. Adjustments have been made for the perforated plate film coefficients taking into account the plate porosity and the heat transfer due to the surface area inside the holes.

The list of temperature runs performed is given in Table A9.1.9-3. This list includes six umbrella thermal transient events given in the design specification as well as stratified flow conditions resulting from forward flushing at 2.7 percent flow.

The forward flushing transient was treated as a steady state solution.

On the basis of the temperature runs, transplots of midpoint-to-edge temperature gradients for the most representative nodes on the welds were obtained. These transplots were used to evaluate the times of severe temperature gradients which can be considered as the times when the largest stresses would occur on the juncture. Figures A9.1.9-13 and A9.1.9-14 depict examples of the transplots.

A9.1.9.7 Thermal Stress Results

All surfaces, excluding the cross sections separating the juncture from the manifold box, were considered as free. The separating cross sections are those sections that connected adjacent areas of the manifold not included in the detailed model. The boundary conditions on the separating surfaces came from the results of the Phase I and Phase III coarse finite element models for each load case (see Section A9.1.5).

Thermal stress runs were performed for the following conditions:

Number	Case	Transient/Steady	Time, sec
			a,c,e
1	RTRIP	Transient	
2	RTRIP	Transient	
3	LSLD	Transient	
4	PLLOAD	Transient	
5	TMHOS	Transient	
6	EXFW	Transient	
7	EXFW	Transient	
8	PLUNLOAD	Transient	
9	FWST 1	Steady	
10	FWST 2	Steady	

Employing the WAPPP computer program, the results of thermal stress calculations were used for the development of 3DCONPLOT's to determine the critical analysis sections and nodes for faulted, maximum range of stress intensity and fatigue evaluations. Examples of the 3DCONPLOT's for different cutting planes in the juncture are given in Figure A9.1.9-15 through A9.1.9-17.

A9.1.9.8 Mechanical Stress Results

Boundary conditions imposed are similar to those for the thermal stress runs. On the separating cross sections, the displacements from the results of the corresponding runs for the coarse finite element model were set, while all other surfaces were considered as free.

The following pressure load cases were evaluated:

Number	Title	Load Case
1	NO	Normal
2	B1	Switchover - With Bypass Flow
3	B2	Switchover - Without Bypass Flow
4	B3	Feedwater Isolation from 100 percent Flow-A
5	B4	Feedwater Isolation from 100 percent Flow-B
6	B5	Excessive Feedwater-A
7	B6	Excessive Feedwater-B
8	B7	Check Valve Closure
9	B81	Check Valve Closure
10	B80	Feedline Break/Check Valve Closure

The details of load cases are given in section A9.1.3. Figure A9.1.9-18 through Figure A9.1.9-20 show examples of the 3DCONPLOT's for several of the pressure load cases.

A9.1.9.9 Evaluation for Faulted Conditions

The feedline break with check valve closure and bubble collapse waterhammer, which give the largest pressure drops at the feedwater nozzle, were considered as faulted conditions. Analyzed were stresses for the feedline break conditions for the flow both out of and into the preheater region. The stresses for the bubble collapse with pressure pulse[ ]a,c,e were obtained by scaling the stresses calculated for the check valve closure event by the ratio of the acoustic ΔP's across the back plate and top/bottom plates.

The following faulted conditions were considered:

Condition	Unit Pressure Load	Scale Factor
		a,c,e
Feedline Break-Flow out of Preheater	B-80	
Feedline Break-Flow into Preheater	B-81	
Bubble Collapse ($+\Delta P$)	B-7	

The darkened lines in Figure A9.1.9-21 through A9.1.9-23 depict the sections in the entrance, exit, and top/bottom plates which were analyzed for faulted evaluations. The faulted evaluations were also performed for sections in the thickness direction of the hole surfaces in the entrance and exit plates (darkened regions in Figures A9.1.9-21 and A9.1.9-22).

Table A9.1.9-4 contains the weld quality factors and fatigue factors for analysis sections. The data is based on Figure A9.1.9-24 and Table NG-355-1 of Reference A9.1-3.

On the basis of Appendix F of the ASME Code, the primary stress limits are the lesser of 2.4 S_m or 0.7 Su.

According to NB-3213.8 (Reference A9.1-3), for the analysis sections, only primary local stresses P_L were considered.

The allowable stress intensities for faulted conditions for each set of the analysis sections are given in Table A9.1.9-5.

The faulted evaluations were performed using the WECEVAL computer program. The highest P_L stresses for WELD 1, WELD 2, WELD 3, and Hole Surface Sections are given in Table A9.1.9-1.

As can be seen, under the loads imposed on the juncture, the welds and the hole boundaries meet the ASME Section III limits.

A9.1.9.10 Maximum Range of Stress Intensity and Fatigue Evaluations

For the maximum range of stress intensity and fatigue evaluations, the normal and upset load conditions considered in the present Section A9.1.9 are given in Table A9.1.9-6.

These conditions are based on the data in Tables A9.1.3-2, A9.1.3-13, and A9.1.3-14. Scale factors on thermal stresses for some of load conditions were determined by the analysis of the actual ΔT and the ΔT at the time thermal stresses were calculated.

The values for Sm and E_{curve}/E_{actual}, for maximum range of stress intensity and fatigue evaluations in the WECEVAL computer program, were taken as 23.3 KSI and 0.8713, respectively.

Maximum range of stress intensity and fatigue evaluations were performed for the Center and Bottom Box Manifold Junctures.

The corner and crossed nodes of the darkened sections shown on Figures A9.1.9-21 and A9.1.9-22 are the nodes analyzed. Considered also were the nodes on the boundaries of the darkened holes, as well as the midpoint "quadratic" nodes in the thickness direction of the top plate (see Figure A9.1.9-23).

a,c,e

Table A9.1.9-2 contains the highest calculated values of the cumulative usage factor for each set of analysis sections.

In all cases, the cumulative usage factor is less than 1.0.

[ ]a,c,e

In all cases, the ratio "maximum range of stress intensity" and cumulative fatigue usage factor cannot exceed 1.0. Hence, the back plate/entrance plate/exit plate juncture of the Model D3 Internal Manifold satisfy the ASME Section III Code allowables for Maximum Range of Stress Intensity and Fatigue Evaluations.

A9.1.9.11 Manifold Flow Guides

The manifold flow guides are internal to the manifold at the outer end of each manifold box, located between the entrance and exit plates. Their purpose is to direct the flow to the outer (curved) end of the exit plate and thereby spread the flow over a greater region of the steam generator tubes.

The flow guides are positioned in the manifold by plug welds to the top and bottom of the exit plate/entrance plate which forms the top and bottom of each manifold.

Mechanical loads are applied to the flow guides by hydraulic forces from feedwater flow through the manifold. Stresses in these components were calculated by the finite element analytical model of the manifold for the appropriate steady state and transient conditions.

Thermal conditions are applied to the flow guides by temperature differences within the manifold and by temperature differences inside and outside of the manifold. These are caused by thermal transients, since under steady state conditions the temperature differences will be negligible. The differential temperatures during the appropriate transients were calculated by the finite element analytical model Stresses were then calculated for these differences by assuming that the flow guides were constrained by the exit and entrance plates. The greatest flow guide temperature on the center line between the plug welds was used in these calculations since this results in conservative stress solutions.

The limiting area to resist mechanical and thermal stresses is the shear area of the plug weld. Worst case as-built tolerances were used for evaluation.

The flow guides were evaluated to Subsection NG of the ASME Boiler and Pressure Vessel Code which specifies that the allowable limits on Stress intensities will be raticed by a Quality Factor which is determined by the type of weld and type of inspection. The Code also specifies that fatigue will be evaluated by multiplying the range of stress intensities by a factor which also is based on weld type and inspection.

The flow guides met the appropriate Code limits on primary shear stress, primary stress intensities, and primary plus secondary range of stress intensities. The fatigue usage factor for all significant thermal and pressure transients is [ ]a,c,e

TABLE 9.1.9-1

RESULTS OF FAULTED EVALUATIONS

Section	Location	Calculated Maximum Stress Intensity, KSI	Allowable Stress Intensity KSI	Calculated S.I./ Allowable S.I.

a,c,e

TABLE 9.1.9-2

RESULTS OF MAXIMUM RANGE OF STRESS INTENSITY AND FATIGUE EVALUATIONS

Section	Location	Maximum Range of Stress Intensity $3 S_m$	Maximum Cumulative Fatigue Usage Factor

a,c,e

TABLE 9.1.9-3

SUMMARY OF THERMAL TRANSIENTS EVALUATED

Number	Title	Version	Transient/Steady	Box Considered
1	RTRIP	Reactor trip from full power with cooldown and steam injection	Transient	a,c,e
2	LSLD	Large step load decrease with steam dump	Transient	
3	PLLOAD	Plant loading at 5 percent of full power/minute	Transient	
4	TBHOS	Two banks of feedwater heaters out of service	Transient	
5	EXFW	Excessive feedwater flow	Transient	
6	PLUNLOAD	Plant unloading at 5 percent of full power/minute	Transient	
7	FWST1	Forward flushing,2.35% Flow Stratification	Steady	
8	FWST2	Forward flushing,2.35% Flow Stratification	Steady	

TABLE 9.1.9-4

ANALYSIS SECTION CLASSIFICATIONS

a,c,e

TABLE 9.1.9-5

ALLOWABLE STRESS INTENSITIES

FOR FAULTED CONDITIONS

Section	Location	Primary Local Membrane, KSI

a,c,e

TABLE 9.1.9-6

NORMAL AND UPSET CONDITIONS

a,c

Number	Load Condition	Cycles	Pressure Case	Scale Factor	Thermal Case	Scale Factor
1	Switchover with Bypass During Unload (+)	458	Switchover (with Bypass Flow)		Unload-1050	
2	Switchover with Bypass During Unload (-)	458	Switchover (with Bypass Flow)		Unload-1050	
3	Switchover without Bypass During Unload (+)	132	Switchover (without Bypass Flow)		Unload-1050	
4	Switchover without Bypass During Unload (-)	132	Switchover (without Bypass Flow)		Unload-1050	
5	Switchover During Load (+)	1550	Switchover (with Bypass Flow)		Stratification	
6	Switchover During Load (-)	1550	Switchover (with Bypass Flow)		Stratification	
7	Switchover During LSLD (+)	200	Switchover (with Bypass Flow)		Unload-1050	

TABLE [illegible].9-6

NORMAL AND UPSET CONDITIONS

(Continued)

Number	Load Condition	Cycles	Pressure Case	Scale Factor	Thermal Case	Scale Factor
8	Switchover During LSLD (-)	200	Switchover (with Bypass Flow)	a,c,e	Unload-1050	a,c,e
9	Feedwater Isolation A (+)	265	Feedwater Isolation from 100 Percent Flow - A		Unload-1050	
10	Feedwater Isolation A (-)	265	Feedwater Isolation from 100 Percent Flow - A		Unload-1050	
11	Feedwater Isolation During Upset Events (+)	470	Feedwater Isolation from 100 Percent Flow - A		LSLD-60	
12	Feedwater Isolation During Upset Events (-)	470	Feedwater Isolation from 100 Percent Flow - A		LSLD-60	
13	Feedwater Isolation During Reactor Trip (+)	30	Feedwater Isolation from 100 Percent Flow - A		R.TRIP-160	

TABLE 9.[illegible].9-6

NORMAL AND UPSET CONDITIONS

(Continued)

a,c,e

Number	Load Condition	Cycles	Pressure Case	Scale Factor	Thermal Case	Scale Factor
14	Feedwater Isolation During Reactor Trip(-)	30	Feedwater Isolation from 100 Percent Flow - A		R.TRIP-160	
15	Feedwater Isolation from 100 Percent Flow - B (+)	5	Feedwater Isolation from 100 Percent Flow - B		Unload-1050	
16	Feedwater Isolation from 100 Percent Flow - B (-)	5	Feedwater Isolation from 100 Percent Flow - B		Unload-1050	
17	Excessive Feedwater Waterhammer A (+)	29	Excessive Feedwater - A		---	---
18	Excessive Feedwater Waterhammer A (-)	29	Excessive Feedwater - A		---	---
19	Excessive Feedwater Waterhammer B (+)	1	Excessive Feedwater - B		---	---

TABLE [illegible]1.9-6

NORMAL AND UPSET CONDITIONS

(Continued)

Number	Load Condition	Cycles	Pressure Case	Scale Factor	Thermal Case	Scale Factor
20	Excessive Feedwater Waterhammer B (-)	1	Excessive Feedwater - B		a,c,e ---	---
21	Check Valve Closure (+)	10	Check Valve Closure		---	---
22	Check Valve Closure (-)	10	Check Valve Closure		---	---
23	Upset Bubble Collapse (+)	10	Check Valve Closure		---	---
24	Upset Bubble Collapse (-)	10	Check Valve Closure		---	---
25	Load	13,200	Normal Operating		Load-284	a,c,e
26	Unload	12,230	Normal Operating		Unload-1050	
27	Forward Flushing A	358	---	---	Stratification	

TABLE [illegible]1.9-6

NORMAL AND UPSET CONDITIONS

(Continued)

Number	Load Condition	Cycles	Pressure Case	Scale Factor	Thermal Case	Scale Factor
				a,c,e		a,c,e
28	Forward Flushing B (LSLD)	103	---	---	Stratification	
29	Forward Flushing C	103	---	---	Stratification	
30	Forward Flushing D	200	---	---	Stratification	
31	Forward Flushing E	223	---	---	Stratification	
32	Forward Flushing F	563	---	---	Stratification	
33	Forward Flushing G	500	---	---	Stratification	
34	100% Power	13,200	Normal Operating		Unload-1050	
35	Reactor Trip	30	Normal Operating		R.TRIP-68	
36	Large Step Load Decrease	200	Normal Operating		LSLD-60	

TABLE 9[illegible]9-6

NORMAL AND UPSET CONDITIONS

(Continued)

Number	Load Condition	Cycles	Pressure Case	Scale Factor	Thermal Case	Scale Factor
37	Heaters Out of Service	360	Normal Operating	a,c,e	TBHOS-626	a,c,e
37a	Heaters Out of Service	360	Normal Operating		EXFW4 (1)	
38	Excessive Feedwater - 1	30	Normal Operating		EXFW1	
38a	Excessive Feedwater - 1	30	Normal Operating		EXFW4	
39	Excessive Feedwater - 2	30	Normal Operating		EXFW4	
40	Upset Thermal Transients	470	Normal Operating		LSLD-60	
41	0% Power	500	---	---	---	---

(1) When considering analysis sections in the Top/Bottom Plates.

a,c,e

THESE FIGURES ARE CONSIDERED PROPRIETARY IN THERE ENTIRITY

FIGURES 9.1.9-1 to 9.1.9-5 DETAILS OF STEAM GENERATOR

FIGURES 9.1.9-6 to 9.1.9-10 FINITE ELEMENT MODELS

a,c,e

THESE FIGURES ARE CONSIDERED PROPRIETARY

IN THERE ENTIRITY

FIGURES 9.1.9-11 TO 9.1.9-12 FINITE ELEMENT MODEL

FIGURES 9.1.9-13 TO 9.1.9-20 CONTOUR PLOTS OF PRESSURE STRESSES

a,c,e

THESE FIGURES ARE CONSIDERED PROPRIETARY
IN THERE ENTIRITY

FIGURE 9.1.9-21 TO FIGURE 9.1.9-24
SECTIONS ANALYZED FOR FAULTED AND
FATIGUE EVALUATIONS.

A9.1.10 Middle Box Exit Plate Flow Splitter Region

A9.1.10.1 Introduction

[

]^{a,c,e} For this reason, a detailed finite-element analysis of the region was undertaken. This region, outlined in Figure A9.1.10-1, was analyzed for various mechanical and thermal load cases. Results were assessed for maximum range of stress intensity, and fatigue. The faulted condition is evaluated in Section A9.1.6.6.

A9.1.10.2 Summary of Results

The centermost portion of the manifold center box was evaluated for maximum range of stress intensity and fatigue. Results are summarized in Tables A9.1.10-1 and A9.1.10-2. In all cases code allowables are satisfied.

A9.1.10.3 Material Properties

This portion of the manifold center box is made of one material,[ ]^{a,c,e} The perforated exit plate region was represented as an equivalent solid material. Adjustments were made to the mechanical and thermal properties of the solid material, consistent with those described in Section A9.1.6 and A9.1.7, to represent that region as an equivalent solid plate. Temperature dependent material properties, given in Section A9.1.2, were used in all analyses for both solid and equivalent plate materials.

A9.1.10.4 Mechanical Loads and Thermal Conditions

The individual loading events can be categorized as either mechanical or thermal. Mechanical loads, summarized in Tables A9.1.3-3 through A9.1.3-12, consisted of pressure loads on the various surfaces of the manifold. Thermal conditions, summarized by the instants of time listed in Table A9.1.10-3, consisted of the most severe temperature distributions that occurred during each of the umbrellaed thermal transients.

A9.1.10-5 Finite-Element Model

A finite-element model of one quadrant of the centermost region of the middle box was constructed with the WECAN computer program. This quadrant model was then reflected into a half model, shown in Figure A9.1.10-2, that consisted of 384 elements. Those elements, WECAN STIF48 (brick) and WECAN STIF55 (wedge), were elastic 3D quadratic isoparametric elements. For the heat transfer analysis, the thermal counterparts of WECAN STIF48 and STIF55, STIF49 and STIF65 respectively, were used.

A9.1.10-6 Boundary Conditions

The thermal boundary conditions applied to the heat transfer model for each of the transients had variable sets of bulk fluid temperatures and heat transfer film coefficients. These sets represented the time and positional variations in feedwater bulk temperatures and film coefficients. When dealing with the perforated exit plate, adjustments had to be made. An equivalent heat transfer coefficient was needed to represent the increased heat transfer due to the surface area inside the holes. This adjustment was consistent with those described in Sections A9.1.6 and A9.1.7.

To analyze the detailed finite-element model for both mechanical and thermal load cases, two types of boundaries were identified. First were the sections of the model that [

]a,c,e The cut-off boundary conditions are displacements from the coarse finite-element model Phase III analyses (see Section A9.1.5). The contact boundary condition are surface tractions from the Phase II manifold box interaction loads converted to pressures and applied to the corresponding locations of the detailed model. The contact boundary condition pressures represent [ ]a,c,e

A9.1.10-7 Heat Transfer Analysis

Results from the six thermal transients were examined to find when the highest stresses occur in each transient. Times were selected when severe temperature gradients exist in the detailed model and when different regions of the detailed model have very different temperatures. For example, Figure A9.1.10-3 shows selected temperatures plotted for the plant unloading transient. All plotted temperatures can be identified as from either solid regions or equivalent solid plate regions. In this particular case the maximum temperature difference in different parts of the structure occurs at [ ]a,c,e

For all transients, the resulting times identifying severe stresses are listed in Table A9.1.10-3. These selected times compare favorably to those independently predicted by the coarse model.

A9.1.10-8 Stress Analysis

A stress analysis was performed for each of the mechanical and thermal load cases using WECAN. Sample results for the large step load decrease thermal case and the check value closure pressure case are shown in Figures A9.1.10-4 and A9.1.10-5, respectively. These figures show results in the form of stress intensity contour plots and structural displacement plots.

A9.1.10-9 Evaluation for Faulted Conditions

The faulted conditions evaluated for the manifold are the feedline break conditions and the bubble collapse waterhammer. These conditions are evaluated in Section A9.1.6.6.

A9.1.10-10 Evaluation for Normal and Upset Conditions

The load conditions considered for the maximum range of stress intensity evaluation and the fatigue evaluation were taken from Tables A9.1.3-2, A9.1.3-13 and A9.1.3-14.

The locations selected for evaluation were based on stress results from the individual load cases, such as those shown in Figures A9.1.10-4 and A9.1.10-5.

The results for the maximum range of stress intensity evaluation are found in Table A9.1.10-1. These results are for the most critical locations. All code allowables are satisfied. All of the locations exclude thermal bending stress per the Simplified Elastic Plastic Method.

The most critical points for the fatigue evaluation are found in Table A9.1.10-2. The results show all usage factors to be below one, so that all code allowables are satisfied.

TABLE A9.1.10-1

SUMMARY OF NORMAL AND UPSET MAXIMUM
RANGE OF STRESS INTENSITY RESULTS

Location	$\frac{P_L + P_b + Q^{(1)}}{3S_m}$

a,c,e

TABLE A9.1.10-2

SUMMARY OF NORMAL AND UPSET FATIGUE RESULTS

Location	Fatigue Usage Factor(1)

a,c,e

TABLE 9.1.10-3

TRANSIENT ANALYSIS TIMES WHEN SEVERE TEMPERATURE GRADIENTS OCCUR

Transient	Transient Times Selected For Stress Evaluation
Plant Loading	
Reactor Trip with Cooldown & S.I.	
Large Step Load Decrease	
Two Banks of Heaters Out of Service	
Excess Feedwater	
Plant Unloading	
Thermal Stratification	

a,c,e

a,c,e

FIGURE 9.1.10-1: [ ]a,c,e ANALYZED WITH DETAILED MODEL

a,c,e

FIGURE 9.1.10-2: CENTERMOST PORTION OF [ ]

a,c,e

THESE FIGURES ARE CONSIDERED PROPRIETARY

IN THERE ENTIRITY

FIGURE 9.1.10-3: TEMPERATURES PLOTTED AT SELECTED LOCATIONS FOR THE PLANT UNLOADING THERMAL TRANSIENT

FIGURE 9.1.10-4: SAMPLE RESULTS FOR LARGE STEP LOAD DECREASE THERMAL CASE EVALUATED THROUGH THE [ ] a,c,e

FIGURE 9.1.10-5: SAMPLE RESULTS FOR CHECK VALVE CLOSURE PRESSURE CASE EVALUATED THROUGH THE [ ] a,c,e

A9.1.11 Threaded Fastener Evaluation

A9.1.11.0 Introduction and Summary

The manifold boxes are connected by a total of 24 threaded fasteners, 12 bolts and 12 tapered studs. The design and materials of these fasteners were carefully selected for the service conditions expected and were chosen on the basis of test data, as explained in Section 5.6. The location of these fasteners is depicted in Figure A9.1.11-1 with the WECAN manifold analysis model utilized in Sections A9.1.6 and A9.1.7. The bolts and studs are labeled with the WECAN model node numbers that will be used throughout this analysis section to designate the fasteners.

The fastener evaluations utilize a combination of conventional, matrix, and finite element analysis methods. Displacements and forces from the WECAN manifold assembly analysis are utilized in the detailed bolt and joint solution to obtain cyclic bolt forces and moments for the stress and fatigue analysis presented in this section. Section A9.1.6.6 provides the stress evaluation for the most critical bolt for Faulted Conditions.

Table A9.1.11-1 provides the summary of results of this evaluation. The stress and fatigue usage are evaluated against the limits of the criteria of the ASME Code, Section III, Subsections NB and NG, and supplemental crack growth analysis, Section 10.0, is provided. [

]a,c,e Preload ranges are as specified in Section 5.0.

A9.1.11.1 Threaded Fastener Geometry and Materials

The geometry of the bolt and stud used is illustrated in Figures A9.1.11-2 and A9.1.11-3, respectively. A full description of the fasteners and preload sequence is contained in Section 5.6.

The bolt, stud, bushing, and nut material is [ ]^{a,c,e} The locking cup and plate material is [ ]^{a,c,e}

A9.1.11.2 Structural Criteria

The criteria for the structural fasteners is that of the ASME Code, Section III, Subsections NB and NG 3230. The criteria is required as a guide only but is satisfied by the analysis except for the supplemental justifications required for bolt No. 7486. The design stress intensity values S_m and yield strength values S_y are from Table I.1 and I.2 of Appendix I of the Code. [ ]^{a,c,e}

A9.1.11.3 Manifold Assembly Interaction Loads

[ ]^{a,c,e}

Loads from the Manifold Assembly analysis for the imposed pressure and thermal transients are summarized in Tables A9.1.6-5 and A9.1.7-1 through A9.1.7-13. These loads were determined using the manifold box interaction analyses presented in Sections A9.1.6 and A9.1.7. The net applied load at each bolt location is given in Table A9.1.11-2 for the thermal conditions. Net applied loads from pressure are all less than [

]^{a,c,e} Loads resulting from seismic events are less severe than for any of the pressure transients. Additional loads, moments and displacements used in individual fastener locations are presented in the evaluation Sections.

A9.1.11.4 Evaluation of Fastener Load Changes

A force-displacement compatibility and equilibrium solution is performed in the bolt configuration using a matrix method of redundant structural analysis. Each of the rotational, shear, and axial degrees of freedom in the bolt, locking cup, nut and plate are incorporated for the bolted joint. In the tapered stud joint, [

]^{a,c,e}

The matrix equation solved in each solution is:

$$\begin{bmatrix} D & P_F^T \\ P_F & 0 \end{bmatrix} \begin{Bmatrix} F \\ \Delta \end{Bmatrix} = - \begin{Bmatrix} e_o \\ P \end{Bmatrix}$$

D = Member Flexibility Matrix

P_F = Member Force Resolution to Nodal Displacements

P_F^T = P_F Transpose

F = Member Forces

Δ = Nodal Displacements

e_o = Member Interferences, Free Thermal Expansions, or Applied Displacements

P = Applied Nodal Forces

Member flexibility δ_{ij} is the deflection in the i direction of the assigned member forces F_i due to a unit load applied at F_j. Applied loads, deflections, or free thermal expansions can be solved through input of the e_o and P matrix. The member force and nodal displacement definition for the bolt joint and stud joint are shown in Figures A9.1.11-4 and A9.1.11-5, respectively. The matrix solution for the bolt joint is given in Figure A9.1.11.6 while the matrix equation for the tapered stud is simply:

$$\begin{bmatrix} \delta_{1\,1} & 0. & -1. \\ 0. & \delta_{2\,2} & -1. \\ -1. & -1. & 0. \end{bmatrix} \begin{Bmatrix} F_1 \\ F_2 \\ \Delta_1 \end{Bmatrix} = - \begin{Bmatrix} e_o \\ e_o \\ P_1 \end{Bmatrix}$$

a,c,e

a,c,e

[ ]^{a,c,e}

where: F = Member Axial Force, pounds

P = Applied Axial Load, pounds

θ = Rotation, radians

ΔT_u = Uniform temperature change, °F

ΔT_{BP} = Temperature difference from bolt to plates, °F

V = Shear force, pounds

M = Bending Moment, inch-pounds

For the stud joint,

[ ]^{a,c,e}

[ ]a,c,e

The matrix method was applied to the model in Figure A9.1.11-7. This represents the location in the region of the bolt at 3582[ ]a,c,e Two cases with only axial flexibility represented and two cases with axial flexibility plus joint bending flexibility were run. One of each was run with double the flexibility of the flange to incorporate the sensitivity to that value. The results given in Table A9.1.11-4 indicate the rotation with joint bending stiffness incorporated is[ ]a,c,e of the value without joint bending stiffness incorporated. In addition, omission of the bending stiffness leads to prediction of gapping at a conservatively low applied load level since the bolt axial load level is conservatively magnified.

The four most critical bolts are:

[ ]a,c,e

The summary of axial load changes and final loads with minimum preload applied is given in Table A9.1.11-5, A9.1.11-6, A9.1.11-7, and A9.1.11-23 for the above bolts, respectively. The bolt relationships previously defined were utilized to arrive at the values listed. The net applied loads are from Table A9.1.11-2. Temperatures and the associated temperature load changes are given in Table A9.1.11-8 and were obtained in the detailed bolt heat transfer solution of Sections A9.1.7 and A9.1.10.

The two most critical studs are:

[ ]a,c,e

The axial loads for the stud at 196 with minimum preload are summarized in Table A9.1.11-9. The stud relationships defined previously were utilized to establish the values given in the table. The net applied axial loads are from Table A9.1.11-2. The temperatures used and associated temperature load changes are given in Table A9.1.11-10. These temperatures are conservatively based on one-dimensional heat transfer solutions for the various transients. The response of the stud was evaluated as one-dimensional from the exposed end. The response of the locking cups and plates were one-dimensional from the exposed surfaces inward. Appropriate thicknesses, boundary conditions, and material properties were used in these evaluations.

In addition to the axial loads for the bolts defined in Tables A9.1.11-5 through A9.1.11-7 and A9.1.11-23, moments or rotations are needed to evaluate the stress cycles used in subsequent fatigue evaluations. Bolt moments for the various events are listed in Table A9.1.11-11. For 256, these bolt moments are obtained from the bolt moment vs. joint moment relationship previously defined and joint moments from the manifold assembly analysis of Section A9.1.7. For 1489, 7486, and 3582, the bolt moments are based on the bolt moment vs. joint rotation relationship previously defined and [ ]a,c,e For 1489 and 7486, the bolt moment [ ]a,c,e

The applied shear loads and required coefficient of friction (with a minimum preload of [ ]a,c,e for each event for bolt 256 is given in Table A9.1.11-12. The maximum required coefficient of friction is [ ]a,c,e This value has been demonstrated by test to be the minimum expected value, Section 5.6.

A9.1.11.5 Stress and Fatigue Evaluation

The axial forces and moments from the previous section are used to evaluate stresses in the fasteners and fatigue usage for the critical threaded sections. For both the stud and the bolt, the stress at the periphery of the threaded section is based on the same section properties used to determine the loads.

Thus,

[ ]a,c,e

In the fatigue usage evaluation, a strength reduction factor of 4.0 is used. No Modulus correction is applied since the same value was used to calculate loads and stresses as is used in the fatigue design curve.

Bearing stress is based on the area under the stud nut or bolt head and compared to the 2.7 S_y limit for [ ]a,c,e using the maximum preload assumption for each fastener. The shear stress in the stud is evaluated at the plate-to-plate interface for the maximum applied shear load of [ ]a,c,e

maximum stud shear stress is [ ]a,c,e

Tables A9.1.11-14 through A9.1.11-17 and A9.1.11-24 provide the summary of fastener stresses at the periphery of the threaded section for the following cases:

Table	Fastener	Condition
-14	Bolt 1489	[ ]a,c,e
-15	Bolt 3582	
-16	Bolt 256	
-17	Stud 196	
-24	Bolt 7486	

Maximum average stress and maximum average plus bending stress is summarized and compared to allowables in Table A9.1.11-18. The allowable for the maximum stress takes account of the higher yield strength (as noted in the footnote) of the purchased material (see Section 5.6). In addition, [

]a,c,e

The fatigue usage calculations for these fasteners for the most severe point at the periphery of the cross section are summarized in Tables A9.1.11-19 through A9.1.11-22 and A9.1.11-25. [

]a,c,e

A9.1.11.6 Conclusions

The threaded fastener evaluation demonstrates that the intent of the ASME Code, Section III, Subsections NB and NG, with supplemental criteria, are satisfied for the conditions of service defined by the specifications of Section 2.0.

TABLE A9.1.11-1

THREADED FASTENER EVALUATION

SUMMARY OF RESULTS

a,c,e

TABLE A9.1.11-2

NET APPLIED TENSILE LOADS AT THE BOLT LOCATIONS

a,c,e

a,c,e

THIS TABLE IS CONSIDERED PROPRIETARY IN ITS ENTIRITY

TABLE 9.1.11-3

MEMBER FLEXIBILITIES FOR THE MATRIX SOLUTION - NON ZERO VALUES

TABLE 9.1.11-4

RESULTS OF BENDING STIFFNESS STUDY

a,c,e

TABLE A9.1.11-5

BOLT AXIAL LOADS AT 1489

Event	Net Applied Load	Applied Load Change		Final Loads(1)	
		Bolt	Plates	Bolt	Plates
Room Temperature					
Hot Shutdown					
Normal Operation					
RT-68					
EXFW-4					
PL-284					
PU-1050					
TBHS-626					
LSLD-60					
Fwd. Fl. (2.7%)					
(2.2%)					
(1.5%)					

a,c,e

TABLE A9.1.11-6

BOLT AXIAL LOADS AT 3582

a,c,e

Event	Net Applied Load	Applied Load Change		Final Loads(1)	
		Bolt	Plates	Bolt	Plates
Room Temperature					
Hot Shutdown					
Normal Operation					
RT-68					
EXFW-4					
PL-284					
PU-1050					
TBHS-626					
LSLD-60					
Fwd. Fl. (2.7%)					
(2.2%)					
(1.5%)					

TABLE A9.1.11-7

BOLT AXIAL LOADS AT 256

a,c,e

TABLE A9.1.11-8

BOLT TEMPERATURE CHANGES AND ASSOCIATED LOAD CHANGES

a,c,e

TABLE A9.1.11-9

STUD AXIAL LOADS AT 196

a,c,e

TABLE 9.1.11-10

[ ] a,c,e TEMPERATURE CHANGES AND ASSOCIATED

LOAD CHANGES

a,c,e

Event
Room Temperature
Hot Shutdown
Normal Operation
RT-68
EXFW-4
PL-284
PU-1050
TBHS-626
LSLD-60
Fwd. Fl. @ 196

[ ] a,c,e

TABLE A9.1.11-11

BOLT MOMENTS

a,c,e

TABLE A9.1.11-12

BOLT SHEAR LOADS AT 256

a,c,e

[ ]

TABLE A9.1.11-13

BEARING STRESS COMPARISON TO

ALLOWABLE FOR THE CRITICAL FASTENERS

a,c,e

TABLE A9.1.11-14

SUMMARY OF STRESSES AT BOLT 1489

a,c,e

(1) The following applies:

1 - Room Temperature/Cold Shutdown (200 cycles).

2 - Hot Shutdown (500 cycles).

3 - Normal Operation.

4 - Reactor Trip (500 cycles).

5 - Excess Feedwater (30 cycles).

6 - Plant Load (13200 cycles).

7 - Plant Unload (12230 cycles).

8 - Two Banks of Heaters out of service (360 cycles).

9 - Large step load decrease (200 cycles).

10 - Forward flushing (2040 cycles).

(2) $F_{Preload} = [\quad]^{a,c,e}$ (minimum).

(3) Refers to sign (+, -) of bending stress.

TABLE A9.1.11-15

SUMMARY OF STRESSES AT BOLT 3582

a,c,e

TABLE A9.1.11-16

SUMMARY OF STRESSES AT BOLT 256

a,c,e

TABLE A9.1.11-17

SUMMARY OF STRESSES AT STUD 196

a,c,e

TABLE A9.1.11-18

CRITICAL FASTENER MAXIMUM STRESS COMPARISON

TO ALLOWABLES

a,c,e

TABLE A9.1.11-19

FATIGUE USAGE AT BOLT 1489

a,c,e

(1) Same as Table 9.1.11-14.

(2) Lower Sign Stresses from Table 9.1.11-14.

(3) <2.7 S_m Fatigue Design Curve.

TABLE A9.1.11-20

FATIGUE USAGE AT BOLT 3582

a,c,e

(1) Same as Table 9.1.11-15.

(2) Upper sign stresses from Table 9.1.11-15.

(3) <2.7 S_m Fatigue Design Curve.

TABLE A9.1.11-21

FATIGUE USAGE AT BOLT 256

a,c,e

(1) Same as Table 9.1.11-16.

(2) Upper Sign Stresses from Table 9.1.11-16.

(3) <2.7 S_m Fatigue Design Curve.

TABLE A9.1.11-22

<u>FATIGUE USAGE</u> [ ] a,c,e

a,c,e

Event Combination (1)
2-5
2-4
3-1
3-8
3-9
3-10

(1) Same as Table 9.1.11-17.

[(2)] a,c,e

TABLE A9.1.11-23

BOLT AXIAL LOADS AT 7486

a,c,e

TABLE A9.1.11-24

SUMMARY OF STRESSES AT 7486

a,c,e

(1) For this stress table:

1 Room Temperature/Cold Shutdown (200 cycles)
2 Hot Shutdown (500 cycles)
3 Normal Operation
4 Reactor Trip (500 cycles)
5 Excess Feedwater (30 cycles)
6 Plant Load (13200 cycles)
7 Plant Unload (12230 cycles)
8 Two Banks of Heaters Out of Service (360 cycles)
9 Large Step Load Decrease (200 cycles)
10A Forward Flushing 1.5% Flow, T_{FW} = 32°F (358 cycles)
10B Forward Flushing 1.5% Flow, T_{FW} = 100°F (103 cycles)
10C Forward Flushing 1.5% Flow, T_{FW} = 150°F (526 cycles)
10D Forward Flushing 1.5% Flow, T_{FW} = 250°F (1063 cycles)

(2) $F_{preload} = [\quad]^{a,c,e}$ (minimum)

(3) Refers to sign (+, -) of bending stress

TABLE A9.1.11-25

FATIGUE USAGE AT BOLT 7486

a,c,e

(1) Same as Table 9.1.11-24

(2) Upper Sign Stresses from Table 9.1.11-24

(3) < 3.0 Sm Fatigue Design Curve

a,c,e

THESE FIGURES ARE CONSIDERED PROPRIETARY

IN THERE ENTIRITY

FIGURE 9.1.11-1 TO 9.1.11-3
MANIFOLD DRAWINGS

a,c,e

[

THESE FIGURES ARE CONSIDERED PROPRIETARY

IN THERE ENTIRITY

]

a,c,e

FIGURE 9.1.11-4: [ ] FORCE AND NODAL DISPLACEMENT

a,c,e

FIGURE 9.1.11-5: [ ] FORCE AND NODAL DISPLACEMENT

a,c,e

THIS FIGURE IS CONSIDERED PROPRIETARY
IN ITS ENTIRITY

FIGURE 9.1.11-6 [ ]^{a,c,e} MATRIX SOLUTION

a,c,e

THIS FIGURE IS CONSIDERED PROPRIETARY
IN ITS ENTIRITY

FIGURE 9.1.11-7: MATRIX SOLUTION MODEL FOR BENDING STIFFNESS STUDY

A9.1.12 Stud/Plate Analysis

A9.1.12.1 Introduction

This Section provides the stress and fatigue evaluation for the interface plates with the tapered studs in the top, mid and bottom sections of the Model D3 Steam Generator internal manifold. The design acceptance criteria for the plates is based on the stress and fatigue limits provided by ASME Pressure Vessel Code Section III Subsection NB and NG. Details of the appropriate limits are provided in Section A9.1.12-2.

There are two interfaces, bottom to mid box and mid to top box. Of the four plates in these intersections the middle box bottom plate was evaluated. The basis of this selection was a differential stud comparison between the two interface locations. Details of the plate selection are provided in Section A9.1.12-3.

The stud/plate stress analysis was based on the solutions obtained from the non-linear finite element model of the internal manifold assembly described in Section A9.1.6 and A9.1.7. From the above model, displacement, force, and temperature boundary conditions were obtained and applied to a more refined finite element model of the plate. Two models were used, the first was a 3D conduction bar model and was used to interpolate the assembly model temperatures to the refined grid, the second was a 3D, 20 node isoparametric solid element model and was used to obtain the stress distribution. Details of the refined thermal and stress finite element models are provided in Section A9.1.12-4.

Stress solutions were obtained for nine thermal conditions. Details of these solutions are provided in Section A9.1.12-5.

Based on the design limits provided in Section A9.1.12-2 and a summary of the stress and fatigue values provided in Section A9.1.12-6, it is concluded that
[ ]a,c,e

A9.1.12-2 Design Criteria

The design acceptance criteria for the plates is based on the guidelines and limits provided in Section III Subsection NB and NG of the ASME Pressure Vessel Code.

a,c,e

The plate material is [ ] The S_m for this material is [ ] a,c,e for all temperatures of interest. The fatigue evaluation was performed using the design fatigue of Figure I-9.2 of Appendix I of the code.

A9.1.12-3 Analysis Methods

The stud interface plate stress evaluation was performed on the bottom plate of the middle box in the assembly. There are two interface regions for consideration. These are between the middle box and either the top or bottom boxes.

a,c,e

[ ]

This table lists nine thermal load conditions, eight of which are symmetric with respect to the top and bottom. The exception is the forward flushing transient where a thermal gradient exists from bottom to top. The net loads for the eight symmetric cases should be identical for the top and bottom interfaces, and with reference to the table they are within a few percent.

The difference is attributed to minor solution inaccuracies. The selection was therefore based on the forward flushing case where the net load at the bottom interface is much larger than at the top.

The specific times in each thermal load case chosen for plate stress evaluation was based on the time in the transient where the stud load was maximum.

Detailed plate stresses were calculated utilizing two refined finite element models and the force, displacement and temperature solutions from the non-linear finite element model of the box assembly. Details of the assembly model are provided in Section A9.1.6 and details of the two refined models are provided in the next section.

Of the two refined models, one was used to provide a temperature solution and the other to use these temperatures and the forces and displacements from the assembly model to calculate stresses. The thermal model consisted of three distinct plans or layers of elements, one layer representing the plate top surface, one for the mid and the third representing the bottom surface. Each of the layers consisted of a refined grid, identical to a surface on the 20 node isoparametric solid element model. The element centroidal temperatures from the assembly model were imposed as nodal temperatures on the conduction plane model and a steady state solution was run, thereby providing interpolated temperatures for the top, mid and bottom surfaces of the 20 node solid grid.

The second refined model consisted of 204, 20 node isoparametric solid elements. (see Figure A9.1.12-1).

[

]a,c,e Displacement boundary conditions were obtained from the assembly model and applied to this model. The displacements at nodes on the boundaries in the refined model which do not correspond to nodes in the assembly model were calculated using a linear interpolation routine.

A9.1.12-4 Finite Element Models

Two finite element models were used to provide refined temperature and stress distributions for the stud interface plates. One model was used to provide the temperature distribution and the other the stress distribution.

The thermal model consisted of three distinct planar finite element grids, representing the top, mid and bottom surfaces of the plate. Each plane was constructed with 3D conduction bars joining the nodal points. The nodal point geometry was identical to the 20 node refined model geometry.

The refined planar finite element grid is shown in Figure A9.1.12-3. This model is constructed of 462 STIF-33 three dimensional conducting bars. Not shown in this figure are the mid side nodes, but there are two conducting bars between each pair of nodes, or for every rectangular element, there are eight conducting bars.

The assembly model course element grid shown in Figure A9.1.12-4 has included bars locating the centroid of the element. An overlay of this grid onto the refined planar grid shown on Figure A9.1.12-5 illustrates the node points in the refined model where the assembly model centroidal temperatures were applied.

The second finite element model used in the stress evaluation is shown in Figure A9.1.12-1. This model is formulated with 204 STIF-48 20 node isoparametric elements. The geometric boundaries of this model and the planar models have the same coordinate locations and axis orientations.

A9.1.12-5 Detailed Stress Solution

The planar models were loaded with all surfaces insulated and with nodal temperatures corresponding to the centroidal temperatures obtained from the solution tapes of the assembly model. A steady state thermal solution was run to provide nodal temperatures for the solid element model. Temperature contour plots of the assembly model and refined model are provided in Figures A9.1.12-6 through A9.1.12-9 for the forward flushing transient. These demonstrate the distributions are very similar.

The refined solid element model utilizes the above temperature solutions as element temperatures. Other loads supplied to the model are listed in Tables A9.1.12-1 and A9.1.12-2. These include axial, shear and moment stud loads and their corresponding reaction loads on the opposite surface. These loads were applied to the model in the following fashion: a,c,e

A stress solution was obtained for each of the load cases listed in Table A9.1.12-1.

The solutions for each of the load cases are illustrated by providing stress intensity contour plots. These are shown in Figures A9.1.12-11 through A9.1.12-19. A listing of the maximum stress intensity ranges in the plate for the load cases are provided in Table A9.1.12-3. These stresses have been linearized through the thickness and adjusted for local plate thickness variations and through thickness thermal bending. The adjustment for thickness variation was accomplished using a factor of $(t_{analysis}/t_{actual})^2$.

a,c,e

[ ]

A fatigue evaluation was performed at various locations in the plate. The evaluation was accomplished using WECEVAL. A summary of the load case combinations and fatigue usage for the worst locations is provided in Table A9.1.12-4.

A9.1.12-6 Summary and Conclusions

A locally refined finite element analysis was performed for the interface plate in the vicinity of the bolts joining top and bottom boxes to the middle box. The analysis included formulation of two refined models of the local area, one model for temperature solutions and the other for stress solutions. The loads and boundary conditions for these local models were obtained from the solution tapes of a non-linear finite element model of the Model D3 internal manifold assembly.

A stress and fatigue evaluation was performed using the limits and guidelines of Section III Subsection NB of the ASME Pressure Vessel Code. The comparison of the plate stresses and cumulative usage to the criteria as provided in Section A9.1.12-2 show [

]a,c,e

TABLE A9.1.12-1

LOADS AT STUD LOCATIONS

a,c,e

Definitions:
- LSLD - Large Step Load Decrease
- TBHS - Two Banks of Heaters Out of Service
- EXFW - Excess Feedwater
- RT - Reactor Trip
- FWD FL - Forward Flushing
- PL - Plant Load
- PU - Plant Unload

(1) For 2.7% flow. These loads represent a conservative set relative to the loads presented in Section 9.1.7 and 9.1.11.

TABLE A9.1-[illegible]2

SHEARS AND MOMENTS [ ]a,c,e

NODE	FORCE	LSLD60	TBHOS626	EXFW4	RTRIP68	PLOAD 284	PUNLOAD 1050	STRAT (FWD. FL.)
177								
196								
199								

]a,c,e

(NOTE Figur 12-20 for Numbered Locations)

TABLE A9.1.12-3

MAXIMUM STRESS INTENSITY RANGES

(Limit = 3Sm = 69.9 ksi)

a,c,e

Transient Combinations	Locations (ksi)											
	1	3*	20	24	36	29	8*	10	11	34**	48	54
AFLUSH-EXFW												
AFLUSH-TBHOS												
AFLUSH-TBHOS												
EXFW-PLOAD												
EXFW-PLOAD												
EXFW-AFLUSH												
AFLUSH-TBHOS												
EXFW-AFLUSH												
EXFW-AFLUSH												
EXFW-AFLUSH												
EXFW-UNLOAD												
EXFW-UNLOAD												

TABLE A9.1.12-4

TRANSIENT COMBINATIONS AND CUMULATIVE USAGE

TRANSIENT SUMMARY

LOAD CONDITION VS SPECIFIED CYCLES

Load Condition Index	Load Condition Notation	Specified Cycles
1	EXFW4	30
2	PLOAD284	13200
3	RTRIP68	30
4	NOROP	13200
5	SHTDWN	500
6	PUNLOAD105	12230
7	LDSW60	200
8	TBHOS626	360
9	A FLUSH	179
10	B FLUSH	52
11	C FLUSH	52
12	D FLUSH	100
13	E FLUSH	112
14	F FLUSH	282
15	G FLUSH	250
16	UPSET TH	470

TABLE A9.1.9-4 (Cont.)

FATIGUE CALCULATIONS
SUMMARY SHEET

Location 519 (8)
Material =[ ]a,c,e

Load Cond Comb	Usable Cycles M	Stress Intensity Range K * SIJ (psi)	Alternating Stress Intensity KE*K*SIJ/2 (psi)	Allowable Cycles N	Usage Factor M/N
1-4*					
4-9*					
4-10*					
4-12*					
4-11*					
4-7*					
4-13*					
4-14*					
4-16*					
4-15*					
3-4*					
4-6*					
5-6					
6-8					

a,c,e

TABLE A9.1.9-4 (Cont.)

(NOTE: The following locations require a [ ]a,c,e

Fatigue Calculations
Summary Sheet

Location 353 (46)
Material = [ ]a,c,e

Load Cond Combo	Usable Cycles M	Stress Intensity Range K * SIJ (psi)	Alternating Stress Intensity KE*K*SIJ/2 (psi)	Allowable Cycles N	Usage Factor M/N
1-9					
4-9*					
4-10*					
4-11*					
4-12*					
4-13*					
4-14*					
4-15*					
4-8*					
4-7*					
3-5					
5-16					
2-4					
2-6*					

a,c,e

Fatigue Calculations
Summary Sheet

Location 354 (4-8)
Material = [ ]a,c,e

Load Cond Comb	Usable Cycles M	Stress Intensity Range K * SIJ (psi)	Alternating Stress Intensity KE*K*SIJ/2 (psi)	Allowable Cycles N	Usage Factor M/N
1-9					
3-9					
9-16					
[illegible]-16					
[illegible]-16					
12-16					
7-13					
8-14					
8-15					
7-15					
6-15					
5-16					
[illegible]-6					
[illegible]-6*					
2-4					

a,c,e

The following figures Are Considered Proprietary in their entirity

A9.1-222 TO A9.1-241

A9.1.13 References

A9.1-1 WECAN - Westinghouse Electric Computer ANalysis, User's Manual, 3/30/81.

A9.1-2 ANSYS - Engineering Analysis System User's Manual, Rev. 4, G.J. DeSalvo, J. A. Swanson, 2/1/82.

A9.1-3 ASME Boiler and Pressure Vessel Code, Section III, 1977 Edition.

A9.1-4 DeSantos, D.F., "Added Mass and Hydrodynamic Damping of Perforated Planes Vibrating in Water," Westinghouse R+D Center, 78-1E7-FLUIB-R1 August 9, 1978.

A9.1-5 Meijers, P., "Plates with Doubly-Periodic Pattern of Circular Holes Loaded in Plate Stress or in Bending," ASME First International Conference on Pressure Vessel Technology, Part 1, Design and Analysis, 1969.

A9.1-6 Patton, Kirk T., "Tables of Hydrodynamic Mass Factors for Transitional Motion," ASME Publication 65-WA/UNT-2, June, 1965.

A9.1-7 WAPPP - WECAN Auxiliary Pre and Post Processors, September, 1980.

A9.1-8 WECEVAL - WECan EVALuation User's Manual, J.M. Hall, A.L. Thurman, J.B. Truitt, Sept., 1981.

A9.1-9 FIGURES II User Guide, Rev. 1, 81-7E7-FIGTO-R1, J.W. Morris, M.B. Newman, J.R. Newman, 6/17/81.

A9.2 Flow Splitter Analysis

A9.2.1 Overall Flow Splitter Analysis

0775c/0112c/040783:5 61

A9.2.1 Overall Flow Splitter Analysis

A9.2.1.1 Introduction

This section of the report presents the analysis of the overall flow splitter for both mechanical and thermal conditions. The analysis was conducted using computer aided analysis almost exclusively. The analysis conclusions are provided in Section A9.2.1.2, and a summary of the stress/fatigue results is given in Section A9.2.1.3. Details concerning the finite element models used for this analysis are provided in Section A9.2.1.4. Material properties used for the analysis are discussed in Section A9.2.1.5, and a discussion of the loads is given in Section A9.2.1.6. Results of the heat transfer, thermal stress, and mechanical stress evaluations are given in Sections A9.2.1.7, A9.2.1.8, and A9.2.1.9 respectively. Finally, the fatigue evaluation is presented in Section A9.2.1.10.

A9.2.1.2 Conclusions

As a result of the flow splitter analysis the following conclusions can be made:

1) The fatigue usages for the major structural members, and for the splitter post/vane weld and the vane/ring weld are less than the allowable value of 1.0.

2) The combined fatigue usage evaluation and fracture mechanics analysis (discussed in more detail in Section 10.0) shows that the splitter ring/thermal liner weld will satisfy its intended function for a 40 year service period.

3) The requirements for normal/upset stress limits are satisfied for all locations except those found to behave unrealistically due to the limitations of the finite element type for some events (more discussion is found concerning these areas in Section A9.2.1.3).

4) The faulted loads evaluation shows that the flow splitter and its attachment welds will maintain their structural integrity having satisfied the elastic stress limits of Appendix F of the Code.

A9.2.1.3 Summary of Results

The evaluation of both the mechanical and thermal stresses was performed using the WECEVAL computer program, Reference (9.2-4).

The results of the WECEVAL evaluation are provided in Tables A9.2.1-1 through A9.2.1-3. A summary of the primary plus secondary stresses is given in Table A9.2.1-1 for critical locations. In reviewing the detailed results it was apparent that errors exist in the stress solution for local areas of the splitter post, splitter vane, and vane/splitter ring weld. High stresses normal to free surfaces indicated that the solutions were in error. For all locations these results occur at locations where an element is exposed to fluid on adjacent surfaces. The transient condition resulting in the high stresses is excess feedwater.

In comparing these results to results obtained using a simplified one-dimensional analysis the simplified analysis indicates that the stresses have been over-predicted by the finite element model. Because of the conservative stress predictions, the associated fatigue results will also be conservative. It is expected that a detailed analysis of these areas would show the 3Sm limit to be satisfied, as areas of comparable or greater thickness at other locations in the model have stresses which satisfy the 3Sm limit.

The maximum fatigue usages for the sections analyzed are given in Table A9.2.1-2. The fatigue usage factor for the splitter ring/thermal liner weld is observed to exceed 1.0. [ ]a,c,e The maximum usage factor of [ ]a,c,e represents a conservative fatigue estimate. A large percentage of the fatigue usage [ ]a,c,e is the result of the 13200 plant load/unload events, which are assumed to occur once each day between 100 percent and 15 percent power. In reality only a fraction of the load follow events would cycle to as low as 15 percent power. If this event is assumed to occur every other day, rather than every day, then the 1.27 fatigue usage can be reduced to approximately 0.8.

A fatigue usage of 1.0, using a design fatigue curve, is an indication of crack initiation, which is calculated to occur in approximately [ ] for the ring/liner weld. Additional time is required for crack growth. The crack growth analysis discussed in Section 10 demonstrates that the combined crack initiation and growth period is greater than the analyzed service period of 40 years. This weld is thus concluded to meet the intended design function for the evaluated service period. a,c,e

The stresses resulting from the feedline break/check valve slam faulted analysis are summarized in Table A9.2.1-3.

A9.2.1.4 Finite Element Models

This analysis was conducted using two finite element models. The first model considered a 60-degree sector of the flow splitter and is shown in Figure A9.2.1-1. Designation of the flow-splitter components is given in Figure A9.2.1-2. The modeling of the structural members was done entirely with isoparametric wedge and solid elements. The flow-splitter plate, which is perforated, was modeled as an equivalent solid plate. (A detailed analysis of the splitter plate, in which the holes are modeled, is presented in Section 9.2.2.)

The 60-degree model was used to evaluate the effect of the mechanical pressure loads and the thermal transients (excluding flow stratification) on the flow splitter. For the thermal transients, heat transfer across the hole boundaries was modeled using convection surface elements.

To evaluate flow stratification, the 60-degree model was extended to a one-hundred eighty degree model which is shown in Figure A9.2.1-3. The thermal liner, although included in the model, has not been shown to allow for more visibility of the flow splitter. The analyses assume symmetry conditions about the flow splitter vertical axis.

A9.2.1.5 Material Properties

The material properties are as defined in Section A9.1.2 for each of the flow splitter structural components except the flow splitter plate. Because the splitter plate was modeled as [

]a,c,e

A9.2.1.6 Summary of Loads

A9.2.1.6.1 Mechanical Loads

The mecahnical loads imposed on the flow splitter are as defined in Section A9.1.3.1. The waterhammer pressure loads reduce to a pressure load imposed on the splitter plate. The applicable loads are given in Tables A9.1.3-3 through A9.1.3-12.

A9.2.1.6.2 Thermal Conditions

The thermal events experienced by the flow splitter are of three types, time varying temperature response due to system transients, flow stratification, and thermal striping. The first two types of thermal conditions are considered as a part of this analysis, while thermal striping is treated both in this section and in Section 9.4.2. Section 9.4.2 deals with the fatigue usage contribution of thermal striping alone. This analysis treats the combination of thermal striping with the other system transients.

The thermal transients for which the flow splitter was analyzed have been discussed previously in Sections A9.1.3.2 and Section 8.1.1. The fluid boundary conditions are summarized in Section 8.1.2.

The results of the flow stratification tests have also been discussed in Section 8.1.2. The stratification test results show [

]a,c,e

A9.2.1.7 Heat Transfer Results

A9.2.1.7.1 Analytical Test Models

Two analytical test models were used to assist in the determination of the model refinement necessary to give accurate heat transfer results. The test models were for a cylindrical section having a radius and thickness comparable to the thermal liner. The transient selected for the test case was excessive feedwater as this is the most severe transient for the flow splitter. (This does not include flow stratification which is essentially a steady state thermal condition.)

The two test models are shown in Figures A9.2.1-4 and A9.2.1-5. The first model is just one element through the thickness, while the second model has two elements in the through-thickness direction. A total of four cases were run. In each case the fluid temperature was varied on the inner and outer surfaces of the thermal liner consistent with the boundary conditions defined in Section 8.2 for this transient.

The first two test cases compared the response of the two models to identical thermal boundary conditions. The resulting thermal responses are shown in Figures A9.2.1-6 through A9.2.1-9. The area of most concern is the accurate prediction of the maximum through-wall gradient. These results show that the two models are within 2-3 percent of each other in predicting the through-wall gradient. It was thus concluded that the model with one-element through the thickness was adequate for the flow splitter analysis.

The remaining cases were run to determine the number of substeps necessary to accurately characterize the thermal transient. For excessive feedwater the fluid is assumed to go from 547°F to 170°F in a period of 1.0 second. Cases 1, 3, and 4 used 100, 50, and 30 substeps respectively during this 1.0 second interval. The results for cases 3 and 4 are shown in Figures A9.2.1-10 through A9.2.1-13. These figures show essentially no change in the maximum calculated through-wall gradient. Thus, for the overall model the first 1.0 second of this transient was divided into 30 substeps.

A9.2.1.7.2 Overall Model Results

This section presents the results of the heat transfer analysis for the seven umbrella thermal transients which were analyzed. Following the completion of each transient run, time varying temperature plots were made. Two types of plots were made. The first represents the actual thermal response with time of the splitter components. The second type of plot displays the time varying temperature difference at a number of locations in the flow splitter.

Plots showing temperatures and temperature gradients for the transient resulting in the highest stresses (excessive feedwater) are shown in Figures A9.2.1-14 through A9.2.1-17. In cases where more than one curve is shown on a plot, the curves represent the thermal response at various locations through a section. In general, the plot showing the most rapid thermal response is located closest to the surface of the component being plotted.

Based on the above plots, a summary has been prepared for each transient showing the largest temperature difference which occurs for the areas plotted, and the time during the transient when the temperature difference occurs. These summaries are shown in Tables A9.2.1-4 through A9.2.1-10. These tables were then reduced to a table showing the times during the various transients that the maximum temperature differences occurred. This summary is shown in Table A9.2.1-11. The times shown in this final table correspond to the points during each transient when stress runs were made.

A9.2.1.7.3 Thermal Stratification Heat Transfer Analysis

This section of the report discusses the effect of flow stratification. The stratification test results from Section 8.1.2 show that there exists a [ ] a,c,e during the steady state condition. To account for the change in the cold water level during the initial part of the forward flushing event, three different levels were considered to be the conditions under which the flow splitter would be subjected to the most severe thermal loads. These three levels are shown in Figures A9.2.1-18, A9.2.1-19 and A9.2.1-20. Figure A9.2.1-18 (Pattern 1) refers to the steady state condition. The stratification layers are divided into three different temperatures, $T_H(\geq 547^\circ F)$ represents the highest temperature, $T_m(\geq 290^\circ F)$ represents the medium temperature, and $T_C(\geq 32^\circ F)$ representing the coldest temperature.

A9.2.1.8 Mechanical Stress Results

For normal/upset mechanical loads the stresses were combined with the associated thermal stresses and compared to the appropriate stress allowables. A summary of these stresses is provided in Table A9.2.1-1. Stresses for each of the waterhammer pressure load cases were determined by scaling results for a unit load case in which a 10 psi pressure drop was assumed to occur across the flow splitter plate. Actual pressure loads for each of the water-hammer events are given in Tables A9.1.3-3 through A9.1.3-12. Stress results for the three seismic loads show the max stresses to be less than 1000 psi.

Stress results for the feedline break/check valve slam loads are provided in Table A9.2.1-3.

A9.2.1.9 Fatigue Results

The fatigue calculations for the flow splitter were performed using the WECEVAL computer program (Reference A9.2-4). Using the WECEVAL program the first step in the evaluation process is to select sections for analysis, assigning each a number. These sections are referred to as ASN's. An analysis section is composed of a string of nodes (from the computer model) through the thickness of a given cross-section.

For the flow splitter, analysis sections were taken through each of the several weld locations and through the thermal liner, splitter ring, splitter post and vanes. Evaluation of the splitter plate was performed using the detailed analysis discussed in Section 9.2.2. The analysis sections chosen for the various welds are shown in Figures A9.2.1-21 through A9.2.1-24 with the corresponding section numbers. At any given location, sections have been taken at a number of circumferential locations, or at several elevations to insure that the area of highest fatigue usage was determined. Analysis sections were also selected at non-weld locations, and the fatigue usage was found to be comparatively low at these locations. The discussion which follows deals principally with the weld locations.

The next step in the analysis process is to determine appropriate mechanical and thermal load combinations. This involves all of the loading conditions discussed earlier. A summary of the load combinations used for the splitter analysis is summarized in Table A9.2.1-12. These load combinations are the result of a review of each transient and the associated system events involved in going from steady state-to-steady state conditions.

Using the guidelines of the ASME Code, Subsection NG, structural discontinuities and welds are treated using the specified fatigue reduction factors. The fatigue reduction factors are applied as stress concentrators to the linearized membrane-plus-bending stress across the section. A summary of the weld quality and fatigue reduction factors used in this analysis are provided in Table A9.2.1-13.

For the flow splitter analysis, the three forward flushing hot/cold interface levels selected for analysis were based on the initial stratification test (2.7 percent flowrate), and engineering judgement as to [

]a,c,e

A summary of the fatigue usages for the three flow levels considered are summarized in Tables A9.2.1-14. A plot of the fatigue usage as a function of flow rate is shown in Figure A9.2.1-25. [

]a,c,e

A summary of the final fatigue usages is provided in Table A9.2.1-2.

Table A9.2.1-1

SUMMARY OF NORMAL/UPSET STRESSES[1]

FOR CRITICAL LOCATIONS

a,c,e

LOCATION	$P_L + P_b + Q$ [2]	ALLOWABLE
		69.90
		67.20
		67.20
		67.20

(1) STRESSES ARE IN KSI.

(2) STRESSES DUE TO THERMAL BENDING HAVE BEEN REMOVED.

Addendum
1-14-83

Table A9.2.1-2

SUMMARY OF FATIGUE USAGES

LOCATION	USAGE	FATIGUE REDUCTION FACTOR

a,c,e

Table A9.2.1-3

SUMMARY OF FAULTED STRESSES(1)

LOCATION	P_m	ALLOWABLE	$P_L + P_b$	ALLOWABLE
	a,c,e			a,c,e
		25.16		37.75
		44.74		67.10
		22.05		33.08
		49.00		73.50
		49.00		73.50
		55.92		83.88
		55.92		83.88

(1) STRESSES ARE IN KSI

Addendum
1-14-83

a,c,e

[Tables 9.2.1-4 to 9.2.1-12 describing temperature differences of various transients and Figure 9.2.1-1 to 9.2.1-23 showing various finite element models and temperature differences of various models and transients are considered Westinghouse Proprietary.]

]a,c,e

Figure 9.2.1-24 ANALYSIS SECTION NUMBERS FOR THE [ ]a,c,e

a,c,e

Figure 9.2.1-25 Fatigue Usage Versus Percent Flow